Geochemistry Geophysics Geosystems G3

Article
Volume 14, Number 10
2 October 2013
doi: 10.1002/ggge.20265
ISSN: 1525-2027

Published by AGU and the Geochemical Society

Chemostratigraphic implications of spatial variation in the Paleocene-Eocene Thermal Maximum carbon isotope excursion, SE Bighorn Basin, Wyoming

Allison A. Baczynski
Department of Earth and Planetary Sciences, Northwestern University, Technological Institute, 2145 Sheridan Road, Evanston, Illinois, 60208, USA (allison@earth.northwestern.edu)

Francesca A. McInerney
Department of Earth and Planetary Sciences, Northwestern University, Evanston, Illinois, USA

Now at Sprigg Geobiology Centre, Environment Institute and School of Earth and Environmental Sciences, University of Adelaide, Adelaide, SA, Australia

Scott L. Wing
Department of Paleobiology, Smithsonian Institution, Washington, D.C., USA

Mary J. Kraus
Department of Geological Sciences, University of Colorado Boulder, Boulder, Colorado, USA

Jonathan I. Bloch
Florida Museum of Natural History, University of Florida, Gainesville, Florida, USA

Doug M. Boyer
Department of Evolutionary Anthropology, Duke University, Durham, North Carolina, USA

Ross Secord
Florida Museum of Natural History, University of Florida, Gainesville, Florida, USA

Now at Department of Earth and Atmospheric Sciences, University of Nebraska, Lincoln, Nebraska, USA

Paul E. Morse
Florida Museum of Natural History and Department of Anthropology, University of Florida, Gainesville, Florida, USA

Henry C. Fricke
Department of Geology, Colorado College, Colorado Springs, Colorado, USA

[1] The Paleocene-Eocene Thermal Maximum (PETM) is marked by a prominent negative carbon isotope excursion (CIE) of 3–5‰ that has a characteristic rapid onset, stable body, and recovery to near pre-CIE isotopic composition. Although the CIE is the major criterion for global correlation of the Paleocene-Eocene boundary, spatial variations in the position and shape of the CIE have not been systematically evaluated. We measured carbon isotope ratios of bulk organic matter ($\delta^{13}C_{org}$) and pedogenic carbonate ($\delta^{13}C_{carb}$) at six PETM sections across a 16 km transect in the SE Bighorn Basin, Wyoming. Bed tracing and high-resolution floral and faunal biostratigraphy allowed correlation of the

sections independent of chemostratigraphy. The onset of the CIE in bulk organic matter at all six sections occurs within a single laterally extensive geosol. The magnitude of the CIE varies from 2.1 to 3.8‰. The absolute and relative stratigraphic thickness of the body of the CIE in bulk organic matter varies significantly across the field area and underrepresents the thickness of the PETM body by 30%–80%. The variations cannot be explained by basinal position and instead suggest that $\delta^{13}C_{org}$ values were influenced by local factors such as reworking of older carbon. The stratigraphic thickness and shape of the CIE have been used to correlate sections, estimate timing of biotic and climatic changes relative to the presumed carbon isotope composition of the atmosphere, and calculate rates of environmental and biotic change. Localized controls on $\delta^{13}C_{org}$ values place these inferences in question by influencing the apparent shape and duration of the CIE.

Components: 13,352 words, 5 figures, 2 tables.

Keywords: Paleocene-Eocene Thermal Maximum; global warming; chemostratigraphy; organic carbon; carbon isotopes; carbon isotope excursion.

Index Terms: 1041 Stable isotope geochemistry: Geochemistry; 1090 Field relationships: Geochemistry; 4806 Carbon cycling: Oceanography: Biological and Chemical; 4870 Stable isotopes: Oceanography: Biological and Chemical; 1605 Abrupt/rapid climate change: Global Change; 4901 Abrupt/rapid climate change: Paleoceanography; 0428 Carbon cycling: Biogeosciences; 0454 Isotopic composition and chemistry: Biogeosciences; 9606 Paleogene: Information Related to Geologic Time.

Received 15 May 2013; **Revised** 27 August 2013; **Accepted** 2 September 2013; **Published** 2 October 2013.

Baczynski A. A., F. A. McInerney, S. L. Wing, M. J. Kraus, J. I. Bloch, D. M. Boyer, R. Secord, P. E. Morse, and H. C. Fricke (2013), Chemostratigraphic implications of spatial variation in the Paleocene-Eocene Thermal Maximum carbon isotope excursion, SE Bighorn Basin, Wyoming, *Geochem. Geophys. Geosyst.*, *14*, 4133–4152, doi:10.1002/ggge.20265.

1. Introduction

[2] The Paleocene-Eocene epoch boundary at ~56 Ma is marked by a significant perturbation to the global carbon cycle. The release of thousands of gigatons of isotopically light carbon to the ocean-atmosphere system resulted in an abrupt, transient episode of extreme global warming known as the Paleocene-Eocene Thermal Maximum (PETM) [*Kennett and Stott*, 1991; *McInerney and Wing*, 2011; *Sluijs et al*., 2007; *Zachos et al*., 1993, 2001]. Mean annual global temperature increased by ~5–8°C during the PETM [*Kennett and Stott*, 1991; *Secord et al*., 2010; *Sluijs et al*., 2006; *Tripati and Elderfield*, 2005; *Weijers et al*., 2007; *Wing et al*., 2005; *Zachos et al*., 2001, 2003, 2005], and in the North American midcontinent the event is concurrent with major changes in faunas [*Gingerich*, 1989, 2003; *Koch et al*., 1992; *Secord et al*., 2012] and floras [*Wing and Currano*, 2013; *Wing et al*., 2005, 2009]. In the marine realm, the PETM carbon cycle perturbation and associated warming are marked by the dissolution of deep marine carbonate due to ocean acidification, the extinction of benthic foraminifers, and an increase in the abundance and geographic range of the dinoflagellate, *Apectodinium* [*Crouch et al*., 2001, 2003; *Sluijs et al*., 2005, 2006; *Thomas*, 1989, 1998; *Zachos et al*., 2005]. The carbon cycle perturbation is recorded in both terrestrial and marine carbonate and organic carbon, plant and algal lipids, and mammalian tooth enamel as a prominent negative carbon isotope excursion (CIE) [e.g., *Bains et al*., 2003; *Bowen et al*., 2001; *Domingo et al*., 2009; *Dupuis et al*., 2003; *Fricke et al*., 1998; *Kennett and Stott*, 1991; *Koch et al*., 1995, 2003; *Magioncalda et al*., 2004; *McInerney and Wing*, 2011; *Pagani et al*., 2006; *Secord et al*., 2010, 2012; *Sluijs et al*., 2006; *Smith et al*., 2007; *Thomas and Shackleton*, 1996; *Zachos et al*., 2005].

[3] The CIE has a characteristic magnitude (~3–5‰) and shape as defined by the duration of the onset (≤20 kyr), body (~100–120 kyr), and recovery (~70–80 kyr) [*Cui et al*., 2011; *Murphy et al*., 2010; *Rohl et al*., 2007]. The exact magnitude and shape of the CIE in atmospheric CO_2 is unknown, and both the magnitude and shape vary according to the environment and material in which the CIE is recorded, diagenesis, and shifts in

depositional rates within local sections [*McInerney and Wing*, 2011]. It is important to understand the factors that influence the shape and magnitude of the excursion in different depositional environments because the CIE is used to correlate continental, transitional, and marine PETM records, develop age models for local sections, and constrain the mechanism and source(s) of carbon release.

[4] The terrestrial record of the CIE in bulk organic matter is predominantly preserved in ancient floodplain depositional environments [*Domingo et al*., 2009; *Magioncalda et al*., 2004; *Manners et al*., 2013; *Schmitz and Pujalte*, 2007; *Thiry et al*., 2006; *Wing et al*., 2005; *Yans et al*., 2006]. Observations of contemporary fluvial systems reveal significant spatial heterogeneity in carbon preservation across the floodplain [*Cierjacks et al*., 2010; *Hill and Cardaci*, 2004; *Hoffmann et al*., 2009; *Samaritani et al*., 2011; *Shrestha*, 2011] and the mixing of carbon from multiple sources (modern and aged plant-derived organic matter and ancient rock carbon) [*Blair et al*., 2010; *Brackley et al*., 2010; *Clark et al*., 2013]. Floodplain environments in the geologic past may have had similar spatial heterogeneity and mixing of carbon from multiple sources that would have affected the isotopic record of bulk organic matter. Preserving an unparalleled record of PETM sedimentary rocks and fossils from ancient floodplain environments, the Bighorn Basin in north central Wyoming provides a unique opportunity to examine how the floodplain environment shapes the expression of the globally recognized CIE associated with the PETM.

[5] In this study we examine the spatial variability in the expression of the CIE in soil organic matter, a material widely used to identify the PETM, at six sites across a 16 km transect in the SE Bighorn Basin, Wyoming (Figure 1). The six sections (HW 16, CAB 10, CAB 3, Big Red Spit, Pyramid Point, and North Butte) have been correlated by physically tracing the surface exposures of marker beds (Figure 2), and correlations are further supported by floral and faunal biostratigraphy identifying the position of the PETM (Figure 3). We also measured the carbon isotope ratios of soil carbonates ($\delta^{13}C_{carb}$) where present. We compare the carbon isotope ratios of bulk organic matter ($\delta^{13}C_{org}$) from these sections with each other and with those from three other Bighorn Basin sections: Polecat Bench [*Magioncalda et al*., 2004], Sand Creek Divide [*Rose et al*., 2012], and Honeycombs [*Yans et al*., 2006]. We consider three main questions: (1) does the onset of the CIE have the same stratigraphic position, magnitude, and thickness across the field area; (2) does the body of the CIE have a uniform thickness and shape across the field area; and (3) what are the implications of this study for chemostratigraphy and our understanding of ecological, evolutionary, and carbon cycle changes at the PETM? The answers to these questions have implications for chemostratigraphic correlation, characterization of the shape of the CIE in relation to time, and understanding how local factors can influence the interpretation of a global event.

2. Study Area

[6] The Bighorn Basin in northern Wyoming preserves a thick sequence of upper Paleocene-lower Eocene continental strata and has been the site of extensive paleontological, sedimentological, and geochemical research on the PETM [*Bowen et al*., 2001; *Clyde and Gingerich*, 1998; *Fricke et al*., 1998; *Gingerich*, 2003; *Koch et al*., 1992, 1995; *Kraus and Riggins*, 2007; *Kraus et al*., 2013; *Magioncalda et al*., 2004; *Rose et al*., 2012; *Secord et al*., 2010, 2012; *Smith et al*., 2007; *Strait*, 2001; *Wing et al*., 2005, 2009; *Yans et al*., 2006]. Abundant exposures and well-understood, high-resolution biostratigraphy make the Bighorn Basin an exceptional setting for examining the influence of local biogeochemical, sedimentological, and environmental factors on the preservation and shape of the CIE.

[7] In the SE Bighorn Basin (Figure 1), the PETM coincides approximately with the transition from the Fort Union Formation (Fm) to the Willwood Fm [*Kraus et al*., 2013; *Rose et al*., 2012; *Secord et al*., 2012; *Wing et al*., 2009]. Both formations are composed largely of mudstone, fine-grained sandstone, and carbonaceous shale. These lithologies are indicative of low-lying floodplain, fluvial channel or channel margin, and abandoned channel depositional environments [*Kraus et al*., 2013; *Wing*, 1998; *Wing et al*., 2005]. Paleosols that formed on fine-grained floodplain deposits are typically drab gray, green, and yellow in the Fort Union Fm but variegated red, purple, and orange in the Willwood Fm as the result of iron oxidation under well-drained conditions [*Kraus and Riggins*, 2007; *Kraus et al*., 2013].

[8] Four informal lithostratigraphic sequences have been recognized in the Paleocene-Eocene rocks of the SE Bighorn Basin [*Kraus et al*., 2013; *Secord et al*., 2012; *Wing et al*., 2009]: (1) a

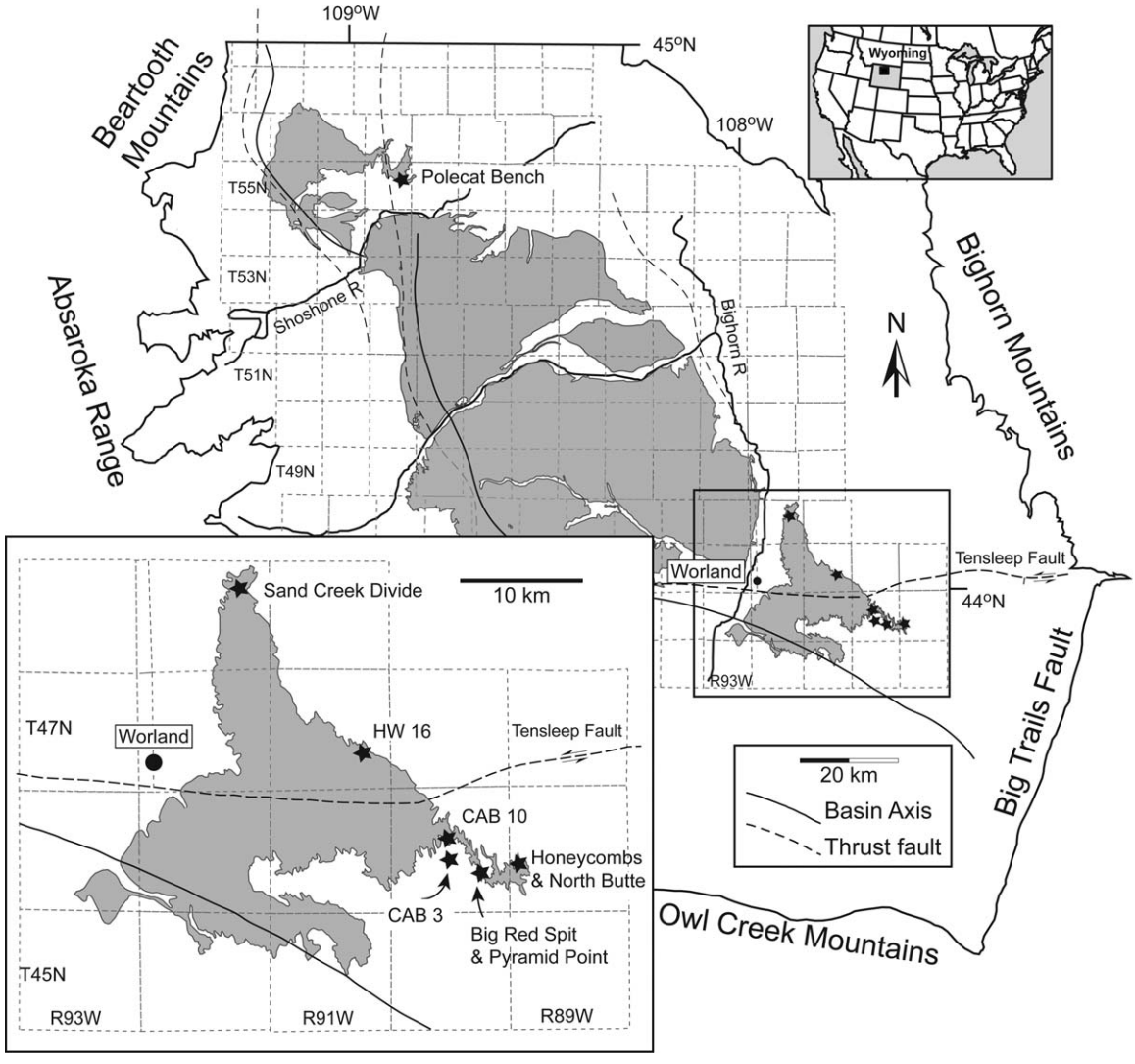

Figure 1. Map showing exposures of the Willwood Formation (shaded) in the Bighorn Basin. Index map in upper right corner shows location of the Bighorn Basin in northern Wyoming. Stars on map and field area inset map mark the locations of PETM sections at Polecat Bench, Sand Creek Divide, HW 16, CAB 10, CAB 3, Big Red Spit, Pyramid Point, Honeycombs, and North Butte. Base map and location of basin axis and Tensleep Fault modified after *Finn et al*. [2010].

"transitional sequence" comprising the uppermost 5–15 m of the Fort Union Fm with localized, purple paleosols; (2) a "lower red sequence" of carbonate-bearing paleosols in the basal 5–10 m of the Willwood Fm that coincides with the onset and early part of the PETM as determined by biostratigraphy (Wa-0 mammalian biozone) and the marked negative shift in $\delta^{13}C$ values of bulk organic carbon, *n*-alkanes [*Smith et al*., 2007], and mammalian tooth enamel [*Secord et al*., 2012]; (3) a "yellow-gray (or cut-and-fill) sequence" ~15 to 20 m thick with weakly developed, yellow-brown paleosols containing large carbonate nodules; and (4) a 15 to 20 m thick "big red sequence" comprised of thick, well-developed, purple and purple-red paleosols that encompasses the uppermost part of the CIE body, all of the recovery phase, and the earliest post-PETM Eocene.

3. Methods

3.1. Bed Tracing

[9] Distinctive and laterally continuous marker beds were tracked on foot across the study area from U.S. Route 16 (HW 16 section) to North Butte (Figure 2). Coordinates were recorded

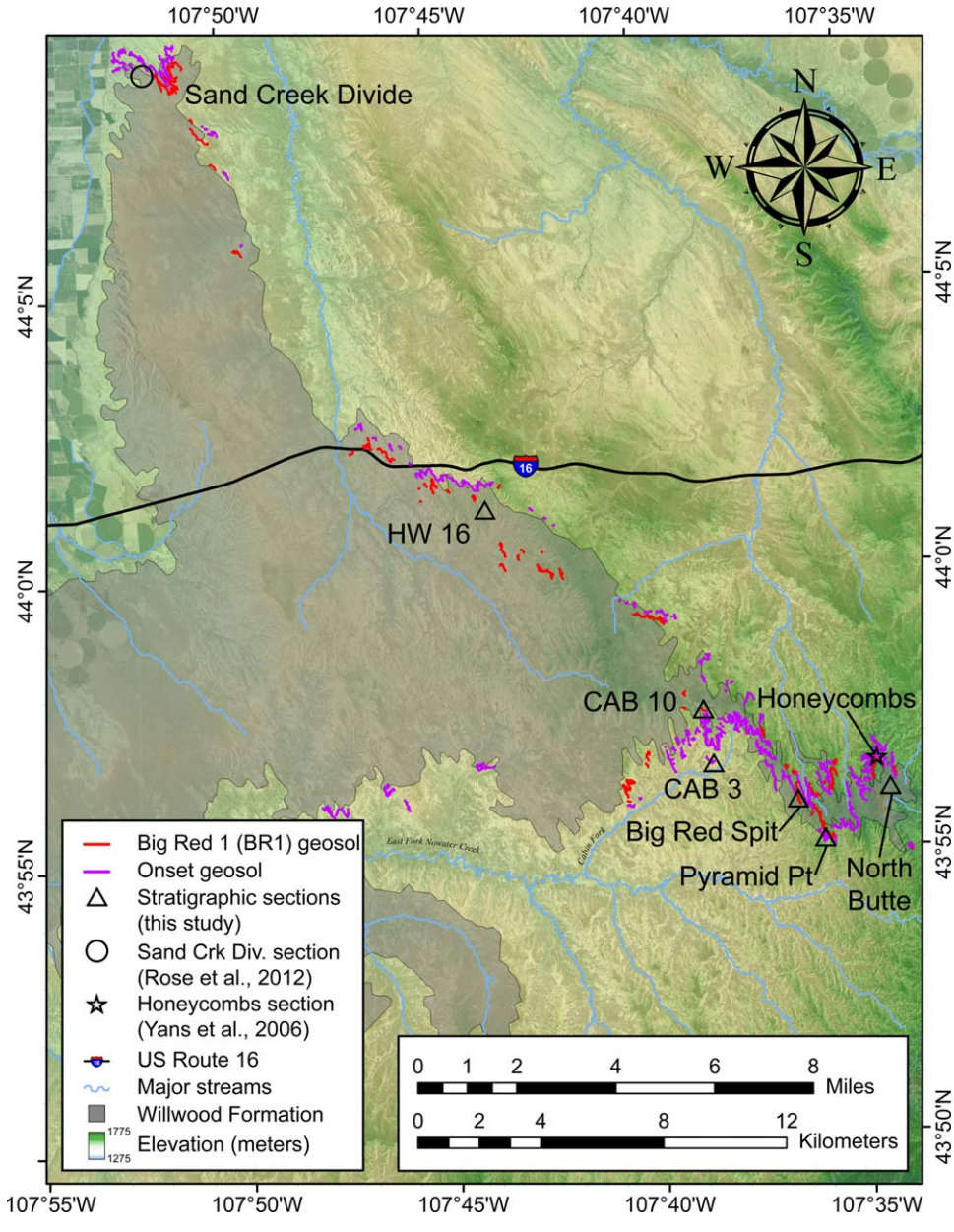

Figure 2. Map of field area in the southeastern Bighorn Basin. Triangles designate locations of detailed stratigraphic sections sampled in this study. Two laterally extensive geosols, the onset geosol and the Big Red 1 (BR1) geosol, were confirmed visually at each location and physically traced between all sites. DGPS points were recorded frequently along the traces and plotted in Google Earth. More detailed bed traces were drawn on high-resolution satellite images in Google Earth using the DGPS data as ground truth (see section 3). Red line represents outcrop trace of the BR1 geosol. Purple line represents outcrop trace of the onset geosol (see text). Map scale is 1:140,000.

frequently along bed traces with a differentially corrected GPS (DGPS: WAAS enabled Trimble ProXRS 2003 model and Trimble Geo-XH 2005 model). Although exposure is not completely continuous, gaps were small enough that bed identity could be confirmed by visual similarity of bed features. The total data set includes 5109 bed points. DGPS coordinates from the bed traces were plotted in Google Earth, and higher fidelity traces of two prominent and laterally extensive marker beds were drawn on high-resolution color satellite images in Google Earth using the coarsely spaced DGPS coordinates as ground truth (Figure 2). Figure 2 shows only a fraction of the tracing data available for assessing bed identity because many other superjacent and subjacent beds were also

traced. Short gaps in beds of interest due to vegetative cover or terrace fill did not necessarily produce uncertainty on bed identity because traceable beds up or down section could be followed until the bed of interest reappeared. DGPS points taken on isolated exposures are not usually represented in Figure 2, as the satellite imagery does not allow extension of those points into linear traces. Additionally, beds in areas of excellent exposure far from measured stratigraphic sections were traced visually, but not always marked by DGPS points, because the exposure was so obvious. DGPS geographic accuracy and precision are submeter. Elevations determined by DGPS are accurate to within 2.5 m relative to the global geoid and also have submeter precision [*Secord et al*., 2012, Supplemental Figure 1]. Using DGPS data to record the difference in elevation between fossil localities and laterally continuous marker beds throughout the field area, we were able to project the relative stratigraphic position of fossil localities onto the nearest measured stratigraphic section (Figure 3).

3.2. Sample Collection

[10] Stratigraphic sections were measured with a Jacob's staff and sighting level after digging ~1 m wide trenches down to fresh, unweathered rock (Figures S1–S6[1]). GPS coordinates were taken at each trench (Table S1). Paleosol field units were designated, and numerous hand samples from each stratigraphic unit were described as outlined in *Kraus et al*. [2013]. Fresh rock samples were collected at high stratigraphic resolution (approximately every 0.25–0.5 m) using a rock hammer and placed in cloth bags for transport and storage. In total, 458 samples were collected from the field area ($n = 127$ at HW 16, $n = 102$ at CAB 10, $n = 24$ at CAB 3, $n = 76$ at Big Red Spit, $n = 14$ at Pyramid Point, and $n = 115$ at North Butte). In situ carbonate nodules were extracted from the rock matrix and collected by stratigraphic level when present. Thirty-two total carbonate nodules were collected from the field area ($n = 12$ at HW 16, $n = 11$ at CAB 10, $n = 6$ at Big Red Spit, and $n = 3$ at North Butte).

3.3. Bulk Organic Matter Sample Preparation and $\delta^{13}C_{org}$ Analysis

[11] Samples were ground to a fine powder with solvent-rinsed mortar and pestle. The powdered sample (1.5 g) was placed in a centrifuge tube; 30 mL of 0.5 *N* hydrochloric acid was added and mixed using a vortex mixer. The acidified samples sat for 30 min to 1 h to remove carbonate, and soluble salts were removed by diluting with deionized water, centrifuging, and decanting until a neutral solution, measured by decanting solution onto pH paper, was achieved. Residues were freeze-dried and powdered again; 5–50 mg of sample (mass of sample calculated based on total organic carbon (TOC) values) was weighed into a tin boat for isotopic analysis. Carbon isotope ratios and weight percent TOC were measured in duplicate using a Costech ECS 4010 combustion elemental analyzer coupled to a Thermo Delta V Plus isotope ratio mass spectrometer (IRMS). Carbon isotope values are reported in delta notation normalized to the international standard Vienna Pee Dee belemnite (VPDB) using acetanilide 1 (Indiana University) and International Atomic Energy Agency (United Nations), Vienna, Austria (IAEA) reference standards 600 and CH-3. Isotope ratios and standard deviations of replicate analyses of standards and samples are reported in Table S1. Replicate measurements of standards indicate a measurement precision of ±0.1‰ ($n = 557$; 1σ). The mean standard deviation on replicate sample analyses is 0.2‰ ($n = 449$).

3.4. Pedogenic Carbonate Sample Preparation and $\delta^{13}C_{carb}$ Analysis

[12] Microsamples of primary micritic calcite from pedogenic carbonate nodules were obtained for stable isotope ratio analysis by drilling on a clean, polished face using a handheld Dremel tool and avoiding secondary diagenetic spar; 250–500 μg of sample was weighed into glass vials and reacted with 100% orthophosphoric acid. The carbon dioxide released by this reaction was purified on a Thermo GasBench II and analyzed on a Thermo Delta V Plus IRMS. Carbon isotope values were measured in duplicate and are reported in delta notation standardized to the VPDB scale using IAEA reference standards NBS-18 and NBS-19. Isotope ratios and standard deviations of replicate analyses of standards and samples are reported in Table S2. Replicate measurements of standards indicate a measurement precision of ±0.1‰ ($n = 16$; 1σ). The mean standard deviation on replicate sample analyses is 0.3‰ ($n = 32$).

4. Results

4.1. Lithostratigraphy

[13] Many marker beds with varying degrees of lateral extent were traced in order to correlate

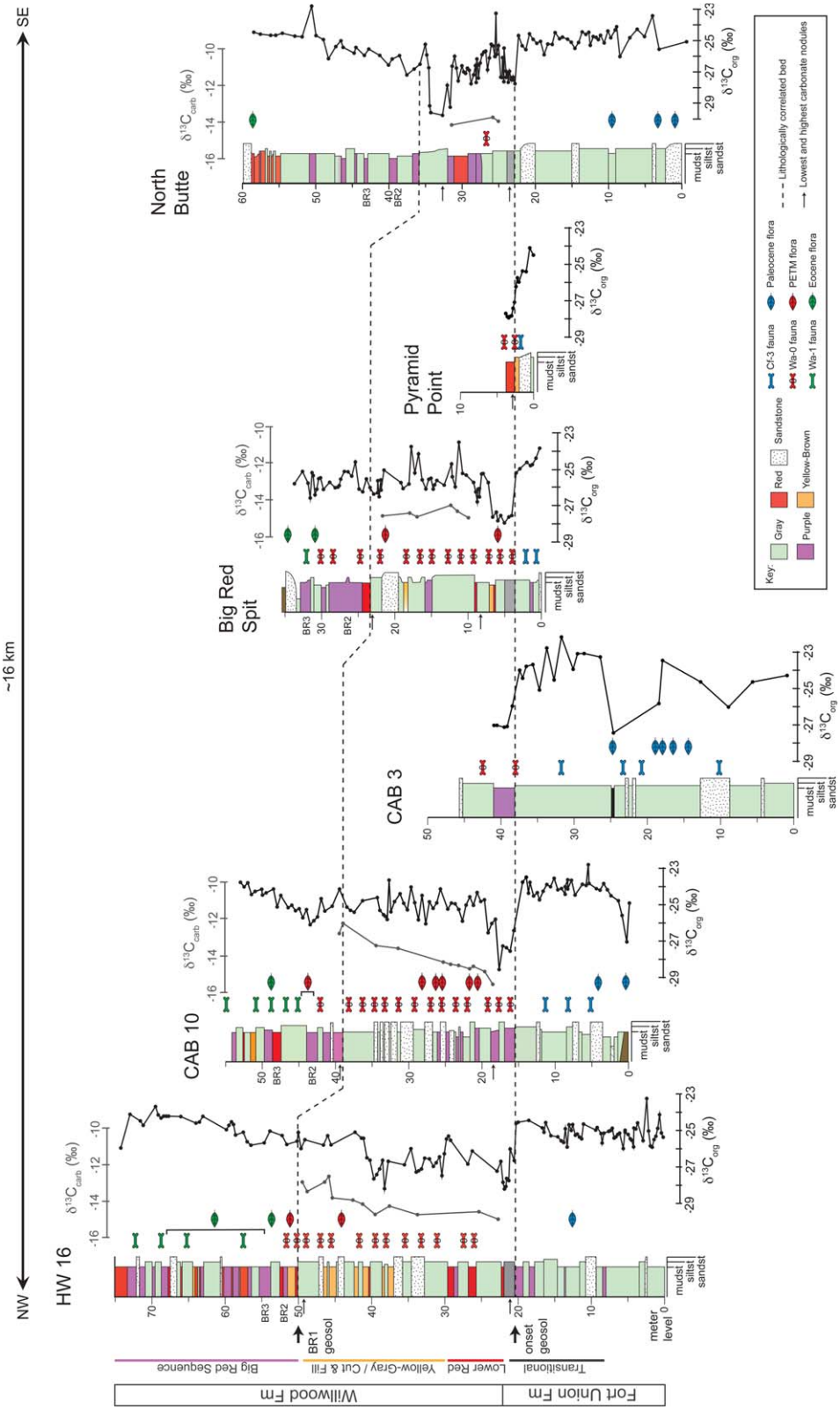

Figure 3. Lithologic sections and bulk soil organic matter (black) and pedogenic carbonate (gray) $\delta^{13}C$ data for HW 16, CAB 10, CAB 3, Big Red Spit, Pyramid Point, and North Butte. Data points represent mean values of replicates (see Table S1). The HW 16 section is divided into four lithologic subdivisions: transitional, lower red, yellow-gray/cut and fill, and big red sequence based on *Kraus et al.* [2013] and *Wing et al.* [2009] and includes the uppermost part of the Fort Union Formation and lowest part of the Willwood Formation. Colors in lithologic sections represent paleosol color. Symbols to the right of lithologic columns denote plant and vertebrate fossil localities. Brackets indicate stratigraphic uncertainty greater than 1 m on plant localities. Black dashed lines represent lithologic correlations based on bed tracing: the lower horizontal dashed line marks the base of the onset geosol, the paleosol containing the stratigraphically lowest excursion $\delta^{13}C$ values; the upper dashed line shows the base of the BR1 geosol, the distinctive brick red paleosol containing a representative Wa-0 fauna and PETM floras. Small black arrows to the left of lithologic columns indicate the lowest and highest stratigraphic levels of carbonate nodules.

adjacent sections and develop a strong lithostratigraphic framework. Most beds are too laterally variable or discontinuous to be traced and/or recognized at every site. However, two prominent, laterally extensive geosols were identified, traced throughout the field area, and used for lithostratigraphic correlation of the six sections (Figure 2). A geosol is defined as a "... laterally traceable, mappable, geologic weathering profile ..." found at a consistent stratigraphic position [*North American Commission on Stratigraphic Nomenclature*, 2005, p. 1560]. We designate the lower prominent geosol as the onset geosol, named for its association with the onset of the CIE, and the upper one as the Big Red 1 (BR1) geosol, named for its position at the base of the big red sequence. We have not formally defined or named these geosols.

[14] Throughout the field area, the onset geosol is unique among uppermost Fort Union Fm and lowermost Willwood Fm paleosols in bearing abundant black, organic fragments. In many locations, it also contains the lowest pedogenic carbonate nodules. The onset geosol varies in color from red to gray. Near U.S. Route 16 (HW 16 section), the onset geosol is gray and lies immediately below the lowest continuous red paleosol (Figure 3). This red paleosol is overlain by another gray bed, forming a gray-red-gray sequence. The gray-red-gray sequence was traced southeast from HW 16 through ~9 km of badland exposure to the north side of the Cabin Fork drainage (CAB 10 section; Figure 2). In the vicinity of CAB 10, the gray-red-gray sequence is not apparent in outcrop, most likely because it is condensed. The red paleosol in the gray-red-gray sequence is expressed as a purple mudstone in the Cabin Fork sections, perhaps because of a change to more poorly drained soil conditions in this area. The stratigraphically lowest carbonate nodules occur a few meters above the base of this purple paleosol at CAB 10. The onset geosol was then traced ~7 km east to the vicinity of North Butte (Figure 2). East of the CAB sections, the onset geosol becomes almost entirely gray in color but still bears black organic fragments and the stratigraphically lowest carbonate nodules. West of CAB 3 and north of the east fork of Nowater Creek, the onset geosol is developed to a moderate degree at the top of a thick sandstone lens, which in turn, is underlain by a ferruginous sandstone containing abundant Paleocene fossils.

[15] The BR1 geosol has also been traced across the study area from HW 16 to North Butte (Figure 2). BR1 is the lowest red bed in a sequence of purple-red beds. It is typically brick red in weathered exposures, is just above the highest pedogenic carbonate nodules, and is usually >1 m thick. Paleosols above the BR1 geosol in the big red sequence are more purple in color and lack carbonate nodules.

4.2. Biostratigraphy

4.2.1. Vertebrate Biostratigraphy

[16] Four mammalian interval biozones are associated with the PETM. From oldest to youngest these zones and their abbreviations (in parentheses) are the *Copecion* (Cf-3), *Meniscotherium priscum* (Wa-M), *Sifrhippus sandrae* (Wa-0), and *Cardiolophus radinskyi* (Wa-1) interval zones [*Gingerich*, 2001; *Secord*, 2008; *Secord et al*., 2006]. The base of each biozone is recognized by the first occurrence of the taxon for which it is named, and the top is defined by the first appearance of the taxon defining the succeeding zone. The *Copecion* zone [*Secord*, 2008; *Secord et al*., 2006], the third and final biozone of the Clarkforkian land-mammal age, is latest Paleocene to earliest Eocene in age. The other three biozones are subdivisions of the Wasatchian land-mammal age, which is earliest Eocene.

[17] *Meniscotherium priscum*, the index fossil for zone Wa-M, occurs in the lowest 4–5 m of the CIE in the northern Bighorn Basin [*Bowen et al*., 2001; *Gingerich*, 2001, 2003; *Gingerich and Smith*, 2006] but is only tentatively documented in the SE Bighorn Basin based on a single specimen found in the Honeycombs area [*Strait*, 2003; *Yans et al*., 2006]. After nine field seasons and the collection of >9000 specimens, no additional *Meniscotherium* specimens have been found in the SE Bighorn Basin. The lack of *Meniscotherium* could be related to sampling or paleoecological biases, or the short interval of time during which it was present in the area might be represented by a hiatus or unfossiliferous rock in some sections.

[18] The *Meniscotherium priscum* zone (Wa-M) is succeeded by the *Sifrhippus sandrae* zone (Wa-0). The Wa-0 biozone is traditionally referred to as the *Hyracotherium sandrae* zone, but "*Hyracotherium*" does not appear to be a valid genus when applied to North American equids [*Froehlich*, 2002]. Thus, we follow the most recent revision of the early Equidae [*Froehlich*, 2002] and refer to the Wa-0 biozone as the *Sifrhippus sandrae* zone. In the SE Bighorn Basin, the base of the Wa-0 biozone corresponds to the onset of the CIE and ends with the first appearance of *Cardiolophus*

radinskyi, the index fossil for biozone Wa-1 (Figure 3).

4.2.2. Floral Biostratigraphy

[19] Two biostratigraphic zones have been described previously for late Paleocene and early Eocene megafloras in the Bighorn Basin: the late Paleocene *Persites-Cornus* Assemblage Zone [*Hickey*, 1980] and the early Eocene *Metasequoia-Cnemidaria* Concurrent Range Zone [*Wing et al*., 1991]. The *Persites-Cornus* Zone corresponds in part to the Clarkforkian land-mammal age, and the *Metasequoia-Cnemidaria* Zone corresponds to mammalian biozones Wa-1 to Wa-4 [*Wing et al*., 1991]. *Persites-Cornus* Zone floras commonly have the conifers *Glyptostrobus* and *Metasequoia*; typical angiosperms include *Davidia antiqua*, *Beringiophyllum cupanioides*, *Browniea serrata*, *Celtis asperum*, *Porosia verrucosa*, and the sycamores *Platanus raynoldsii* and *Macginitiea gracilis*.

[20] No formal biozone has been named for PETM megafloras, but they are almost entirely distinct from those that precede and follow [*McInerney and Wing*, 2011; *Wing and Currano*, 2013; *Wing et al*., 2005]. Only two taxa present in the *Persites-Cornus* Zone are found in the PETM assemblages, which are dominated in diversity and numbers by species in the families Fabaceae (beans) and Arecaceae (palms) [*Wing and Currano*, 2013; *Wing et al*., 2005, 2009]. The floras dominated by beans and palms occur only in faunal biozone Wa-0 (Figure 3). One Eocene index taxon, the floating fern *Salvinia preauriculata*, has its first appearance in the body of the CIE. Conifers and *Ginkgo*, which are otherwise common throughout the late Paleocene and early Eocene, are absent from the PETM.

[21] Conifers and *Ginkgo* reappear in the post-PETM *Metasequoia-Cnemidaria* Zone and are common throughout. Many of the angiosperms present in the late Paleocene also reappear after, or in the recovery phase, of the CIE. *Davidia antiqua*, *Beringiophyllum cupanioides*, *Browniea serrata*, *Celtis asperum*, and *Porosia verrucosa* are, however, absent from the *Metasequoia-Cnemidaria* Zone and may not have returned to the Bighorn Basin following the PETM. Megafossil species with first appearances low in the *Metasequoia-Cnemidaria* Zone include *Alnus* sp., *Platycarya americana*, and the ferns *Cnemidaria magna* and *Lygodium kaulfussi*.

4.3. Integration of Lithostratigraphy and Biostratigraphy

[22] Diverse upper Paleocene floras and a modest assemblage of late Clarkforkian (Cf-3, uppermost Paleocene) mammals have been recovered below the base of the onset geosol (Figure 3) [*Secord et al*., 2012; *Wing et al*., 2005, 2009]. The youngest *Persites-Cornus* Zone floras occur ~8 m below the base of the onset geosol in the HW 16 section, approximately in the middle of the "transitional sequence," and the youngest Clarkforkian mammals are found less than 4 m below the base of the onset geosol at Big Red Spit and Pyramid Point (Figure 3) [*Wing et al*., 2009]. Wa-0 faunas and/or PETM floras with abundant beans and palms appear less than 0.5 m above the base of the onset geosol at CAB 10, CAB 3, Big Red Spit, and Pyramid Point and are present throughout the lower red and yellow-gray (or cut-and-fill) sequences. The BR1 geosol occurs in the upper part of the Wa-0 biozone (Figure 3) [*Secord et al*., 2012; *Wing et al*., 2005, 2009]. PETM floras and Wa-0 mammals are found within and up to a meter above the second purple-red paleosol in the big red sequence (BR2; Figure 3). The lowest stratigraphic occurrence of a *Metasequoia-Cnemidaria* Zone (lower Eocene) flora is in a cut-and-fill deposit between BR2 and the third purple-red paleosol of the big red sequence (BR3) at HW 16 and Big Red Spit (Figure 3). *Cardiolophus radinskyi*, the indicator of biozone Wa-1, also first occurs between BR2 and BR3 (CAB 10) and within a few meters above a shift back to larger body size in the *Sifrhippus sandrae* lineage [*Secord et al*., 2012].

4.4. Carbon Isotope Ratios

[23] The $\delta^{13}C_{org}$ records for the six PETM sections display broadly similar stratigraphic trends (Figure 3). In stratigraphic order these are as follows: (1) an ~20 m thick interval in the uppermost Fort Union Fm with $\delta^{13}C_{org}$ values typically greater than or equal to −25‰; (2) a 1 to 2 m thick interval in the onset geosol in the basal Willwood Fm in which there is a 2–4‰ negative shift in $\delta^{13}C_{org}$ values; (3) an interval of variable stratigraphic thickness in which $\delta^{13}C_{org}$ values are typically less than or equal to −26‰; (4) a return to less negative $\delta^{13}C_{org}$ values of about −25‰; and (5) an interval in which $\delta^{13}C_{org}$ values are generally greater than or equal to −25‰.

[24] We calculate the magnitude of the CIE onset as the difference between the stratigraphically highest $\delta^{13}C_{org}$ value that precedes the onset geosol and the most negative $\delta^{13}C_{org}$ value within the onset geosol. The thickness of the CIE onset is the stratigraphic separation of these points. The magnitude of the CIE onset ranges from 2.1‰ to 3.8‰, and the thickness of the CIE onset interval

Table 1. CIE Onset Magnitude and Thickness, Thickness of CIE Body Based on $\delta^{13}C_{org}$ Values, Biostratigraphic (Wa-0) PETM Body Thickness, $\delta^{13}C_{org}$ CIE Body Incompleteness, Interval Between Onset and BR1 Geosols, and Median of Absolute Differences Between Adjacent $\delta^{13}C_{org}$ and $\delta^{13}C_{carb}$ Samples Within the CIE Body

Site Locality	Onset Magnitude (‰)	Onset Thickness (m)	$\delta^{13}C_{org}$ CIE Body Thickness (m)	Biostratigraphic (Wa-0) PETM Body Thickness (m)	$\delta^{13}C_{org}$ CIE Body Incompleteness (%)[a]	Interval Between Onset and BR1 Geosols (m)	Median Absolute Differences $\delta^{13}C_{org}$ Within CIE Body (‰)	Median Absolute Differences $\delta^{13}C_{carb}$ Within CIE Body (‰)
HW 16	3.6	1.6	21	33	36	30	0.67	0.46
CAB 10	3.8	1.7	5	28.5	82	23	0.58	0.23
CAB 3	3.1	1.7						
Big Red Spit	2.8	1.6	6	27	78	20	0.52	0.32
Pyramid Point	2.1	1						
North Butte	3.1	0.5	12	18	33	13	0.66	0.3

[a] $\delta^{13}C_{org}$ CIE body incompleteness calculated as $1 - \delta^{13}C_{org}$ CIE body thickness/Wa-0 thickness.

varies from 1.7 to 0.5 m (Table 1). The interval of rock with $\delta^{13}C_{org}$ values consistently less than or equal to −26‰ ranges from ∼5 to ∼21 m (Table 1). The median of absolute differences between $\delta^{13}C_{org}$ values of adjacent samples within the excursion is greater than 0.5‰ at each site (Table 1).

[25] New measurements of the $\delta^{13}C$ values of pedogenic carbonate nodules from HW 16, Big Red Spit, and North Butte are presented in gray in Figure 3, along with previously published $\delta^{13}C_{carb}$ data from CAB 10 [*Wing et al.*, 2009]. Small arrows in Figure 3 denote first and last appearances of pedogenic carbonate. Carbonate nodules are present only within the PETM body in the SE Bighorn Basin, and all $\delta^{13}C_{carb}$ values are between −12 and −16‰ (Figure 3). Although the $\delta^{13}C_{carb}$ records do not capture the onset of the CIE, the $\delta^{13}C_{carb}$ values we measured from within the PETM body are comparable to CIE body $\delta^{13}C_{carb}$ values at other Bighorn Basin sites that do preserve the onset and body of the PETM [e.g., *Bains et al.*, 2003; *Bowen et al.*, 2001; *Koch et al.*, 1995, 2003]. The Polecat Bench PETM section has the longest and highest resolution record of pedogenic carbonate $\delta^{13}C$, and sustained $\delta^{13}C_{carb}$ values less than −12‰ are found only within the CIE (Figure 4) [*Bowen et al.*, 2001]. The median of absolute differences between $\delta^{13}C_{carb}$ values of adjacent samples within the excursion is less than 0.5‰ at each site (Table 1).

5. Discussion

5.1. Position, Magnitude, and Thickness of the CIE Onset

[26] Although it is often assumed that the onset of the CIE can be used to correlate different PETM sections, no previous study has demonstrated that this chemostratigraphic marker occurs in the same lithostratigraphic position across an ancient landscape. The lithostratigraphic and biostratigraphic framework we have established in the SE Bighorn Basin allows us to show that across 16 km, the onset of the CIE occurs within the laterally traceable bed we term the onset geosol. The onset geosol has been estimated to represent ∼24 kyr [*Secord et al.*, 2012, LIRB], giving a maximum duration for the onset of the CIE that is consistent with other recent estimates (∼15–25 kyr) [*Bowen et al.*, 2006; *Charles et al.*, 2011; *Cui et al.*, 2011].

[27] The magnitude of the CIE at the six sites ranges from 2.1‰ to 3.8‰ (Table 1). These spatial variations cannot be attributed to incomplete sampling of the CIE because sample resolution is high across the CIE onset (every ∼0.1–0.5 m) and includes multiple samples from within the onset geosol at all localities. Variations in CIE magnitude among sections probably reflect the mixing of carbon from different sources (with different carbon isotope values), or different degradational states of organic matter, rather than incomplete sampling.

[28] The thickness of the CIE onset interval changes abruptly across the study area (Table 1 and Figure 3). It averages 1.65 m (±0.06 standard deviation) to the west but is much thinner at Pyramid Point (1.0 m) and North Butte (0.5 m). Unlike the gradual thinning of the entire PETM sequence from NW to SE (Figure 3 and Table 1), which is consistent with slower long-term depositional rates in that direction [*Bown*, 1980; *Clyde et al.*, 2007; *Kraus*, 1992], the abrupt thinning of the onset across small distances suggests local causes such as small-scale scouring or other floodplain processes.

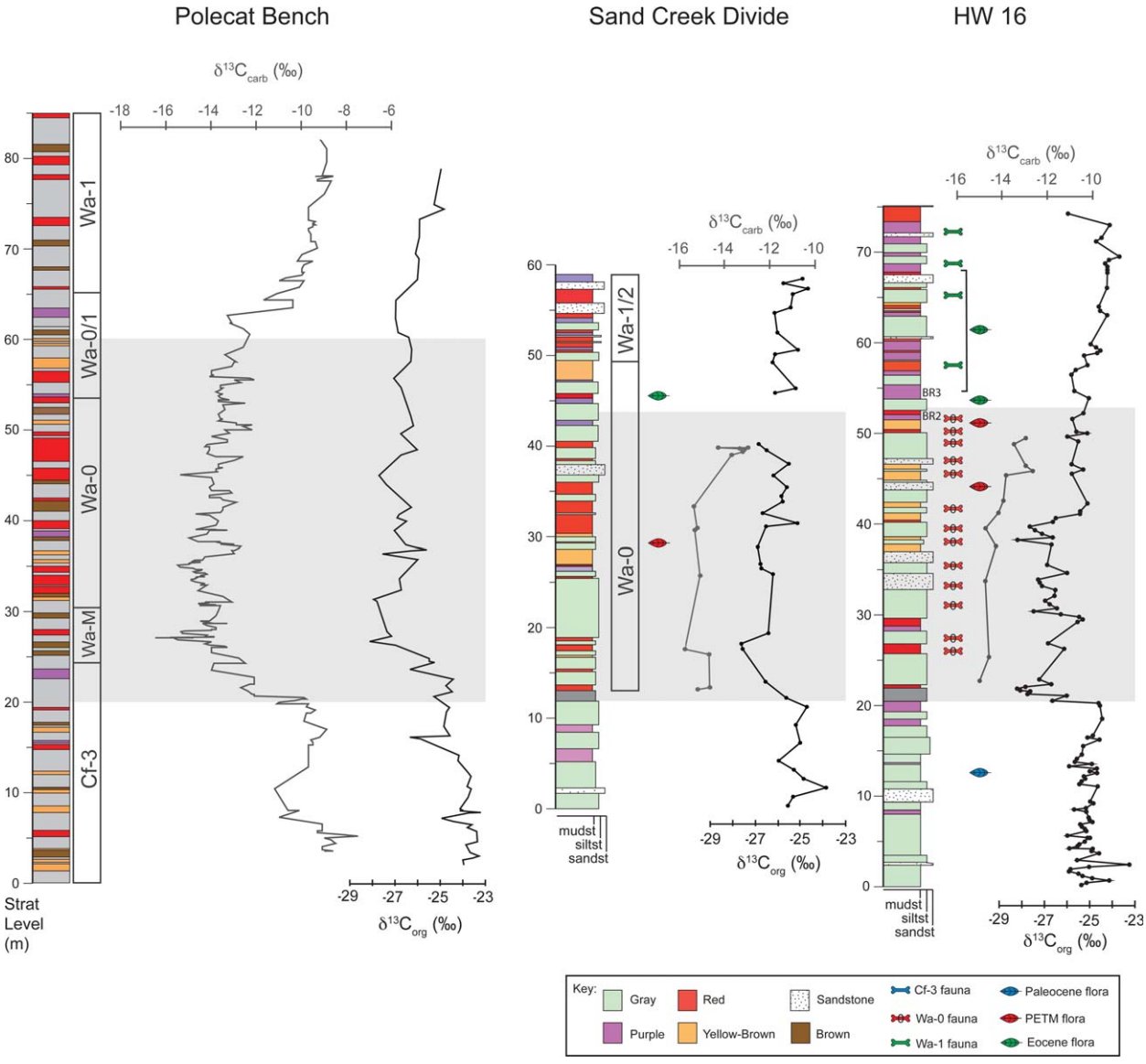

Figure 4. Lithologic sections and bulk soil organic matter (black) and pedogenic carbonate (gray) $\delta^{13}C$ data for Polecat Bench, Sand Creek Divide, and HW 16. Polecat Bench lithologic section modified from *Smith et al*. [2008]; carbon isotope data modified from Figure 3A of *Abdul Aziz et al*. [2008] with the original isotope data for dispersed organic carbon from *Magioncalda et al*. [2004] and pedogenic carbonate (three point moving average) from *Bowen et al*. [2001]. Gray box indicating PETM interval at Polecat Bench based on *Smith et al*. [2008], as defined by vertebrate biostratigraphy and carbon isotope excursions. Sand Creek Divide vertebrate biostratigraphy from *Rose et al*. [2012]; lithologic section and carbon isotope data modified from *Rose et al*. [2012]. Gray box indicating PETM interval at Sand Creek Divide is consistent with distribution of vertebrate and plant fossil localities.

5.2. Variability in the Thickness and Shape of the CIE Body

[29] The stratigraphic thickness of the interval with excursion $\delta^{13}C_{org}$ values ($\delta^{13}C_{org} < -26‰$) varies widely among our sites and does not thin in parallel with the gradual NW to SE thinning of the interval between the onset and BR1 geosols (Figure 3 and Table 1). Rather than maintaining a consistent relationship to the traced geosols, the return to less negative $\delta^{13}C_{org}$ values occurs at a different relative stratigraphic position in each section. The lack of consistency in the relative position of the tops of the excursion intervals in different sections implies that they are not contemporaneous and cannot all record the full duration of the PETM body.

[30] Biostratigraphic and isotopic records suggest that none of the bulk organic matter records presented here record the full duration of the body of the PETM. Fossil and isotopic evidence indicates that the PETM body persists from the base of the onset geosol to at least BR2. Wa-0 fossils, which occur only within the PETM body, are found from the onset geosol to ~1 m above the top of BR2 (Figure 3). Stable carbon isotope measurements from both tooth enamel and leaf wax lipids [*Secord et al*., 2012; *Smith et al*., 2007] also indicate that the PETM body extends from the base of the onset geosol to at least BR2. Pedogenic carbonate nodules record excursion values ($\delta^{13}C_{carb} < -12‰$) to at least BR1, above which carbonate nodules are no longer found (Figure 3). In contrast, $\delta^{13}C_{org}$ values return to preexcursion values ~6–24 m below where tooth enamel and leaf wax lipid $\delta^{13}C$ values return to preexcursion values and where the transition from Wa-0 to Wa-1 mammals occurs. Therefore, in our field area, the CIE observed in bulk organic matter underrepresents the thickness of the PETM body by 30–80% (Table 1).

[31] We propose that the large variation in the shape and thickness of the body of the CIE measured in bulk organic matter results from the mixing of different pools of carbon: autochthonous carbon fixed during the PETM and allochthonous carbon eroded from pre-PETM soils or rocks. The premature return to less negative $\delta^{13}C_{org}$ values could be explained by an increase in the proportion of reworked (^{13}C-enriched) allochthonous carbon, either due to an increase in the input of allochthonous carbon or to a decrease in the production and/or preservation of autochthonous carbon. The presence of older, refractory carbon has been observed in palynological preparations of PETM rocks from the study area [*Wing et al*., 2005, supplement]. Shark teeth and dinoflagellates found in terrestrial PETM sediments throughout the field area and Cretaceous zircons found in the CAB 10 section also suggest the introduction of allochthonous Mesozoic material.

[32] Studies conducted in modern fluvial systems have shown that refractory (rock) carbon is found in both riverine and floodplain sediments. In modern systems, the concentration of rock carbon remains relatively constant from sedimentary source rock to riverine and floodplain sediments at ~0.25–0.4 weight percent [*Blair et al*., 2010; *Clark et al*., 2013] and can constitute up to 80% of the particulate organic carbon pool [*Clark et al*., 2013]. Paleocurrent studies of Willwood strata in the southeastern part of the basin show paleoflow from southeast to northwest [*Neasham and Vondra*, 1972; *Newbury*, 2011; *Seeland*, 1998] and point to the Southern Bighorn Mountains as the likely sediment source for the PETM deposits. The Southern Bighorn Mountains consist of a crystalline core flanked by sedimentary rocks of Paleozoic and Mesozoic age [e.g., *Love and Christiansen*, 1985]. Cretaceous marine units, which form a major part of those strata, contain considerable thicknesses of gray to black shales that are locally carbonaceous [*Eicher*, 1962; *Hagen and Surdam*, 1984; *Keefer*, 1972]. These carbonaceous Mesozoic rocks are enriched in ^{13}C relative to PETM material. Therefore, an increase in the proportion of allochthonous carbon could explain the truncation of the CIE prior to the end of the PETM. Using the most negative PETM bulk organic matter excursion value (−28.5‰) and a mean Mesozoic $\delta^{13}C_{org}$ value (−24.3‰, $n = 10$ formations; Table S3) in a simple binary mixing equation, we calculate that ~40–80% allochthonous carbon would be required to produce the observed premature return to less negative $\delta^{13}C_{org}$ values (see supporting information Table S4)[1]. Similarly high proportions of rock carbon have been found in modern river systems, where rock carbon has been shown to constitute from 30 to 80% of the total particulate organic carbon pool [*Blair et al*., 2010; *Clark et al*., 2013]. Therefore, mixing of allochthonous rock carbon provides a realistic explanation for the truncation of the CIE. However, this mixing calculation represents a conservative lower-bound estimate of the proportion of allochthonous carbon because the true value of PETM bulk organic matter is unknown, and the estimated value of −28.5‰ likely includes some proportion of rock carbon. Additional constraints on the $\delta^{13}C_{org}$ value of PETM bulk organic matter and the provenance of allochthonous carbon would improve this estimate.

[33] Pedogenic processes can also influence organic matter $\delta^{13}C_{org}$ values. Depth profiles in modern soils show a logarithmic relationship between the fraction of soil organic carbon remaining (f_{SOC}) and $\delta^{13}C_{org}$ value: as f_{SOC} decreases, $\delta^{13}C_{org}$ values increase, i.e., become more enriched in ^{13}C due to Rayleigh distillation [*Wynn*, 2007]. A similar logarithmic relationship between weight percent TOC and bulk organic matter $\delta^{13}C$ values has been observed previously

[1]Additional supporting information may be found in the online version of this article.

in Paleogene sediments from this field area [*Wing et al*., 2005] and is also found here (Figure S7). Although decomposition may have played an important role in altering the carbon isotope signature of organic matter in paleosols, attributing the logarithmic relationship in the Paleogene to the same mechanism identified in modern soils relies on an implicit assumption that weight percent TOC is a reliable proxy for f_{SOC}. For this to be true, the initial carbon content of all the sediments must have been the same, which is unlikely. Therefore, although soil organic matter degradation likely influenced $\delta^{13}C_{org}$ values, these effects are difficult to identify in our samples.

[34] A similar pattern of ^{13}C enrichment with decreasing weight percent TOC (Figure S7) could also be caused by the mixing of ^{13}C-enriched allochthonous rock carbon with autochthonous carbon, if the proportion of allochthonous carbon increased with decreasing weight percent TOC. The allochthonous/autochthonous mixing ratio could vary systematically with TOC due to (1) sedimentary processes (e.g., avulsion deposits in the yellow-gray interval with low TOC and likely high allochthonous inputs versus well-developed paleosols with high autochthonous inputs and higher TOC), (2) preservational bias (e.g., preferential preservation of refractory rock carbon relative to PETM carbon in sediments with low TOC), or (3) varying production of organic carbon (e.g., higher relative input of PETM organic matter in higher TOC sediments such as those that preserve fossil leaves). If the allochthonous/autochthonous mixing ratio underlies the relationship between $\delta^{13}C_{org}$ values and TOC, we would predict that PETM sediments should exhibit a larger ^{13}C enrichment with decreasing TOC than pre- and post-PETM sediments. This is because pre- and post-PETM $\delta^{13}C_{org}$ values are similar to Mesozoic $\delta^{13}C_{org}$ values and would therefore be less affected by mixing than PETM $\delta^{13}C_{org}$ values. The data in fact show greater ^{13}C enrichment with decreasing weight percent TOC in PETM samples than in pre- and post-PETM samples (Figure S7), suggesting that mixing of allochthonous and autochthonous carbon could play an important role in shaping these carbon isotope records.

5.3. Implications for Chemostratigraphy and Our Understanding of the PETM

5.3.1. Proximal Correlations: Variability Across the Field Area

[35] This study clearly documents variation in the expression of the CIE in bulk organic matter across 16 km of outcrop. Differences in $\delta^{13}C_{org}$ values within beds traced laterally between sites are on the order of 1–2‰, and the median of absolute differences between successive samples within the body of the CIE at each section is >0.5‰ (Table 1). Variability in $\delta^{13}C_{org}$ values over short stratigraphic and lateral distances is commonly observed in Bighorn Basin Paleogene sections [*Diefendorf et al*., 2007; *Smith et al*., 2007; *Wing et al*., 2005, 2009] and can be attributed to the diversity of organic input to soils, differential preservation/degradation of organic components, and isotopic effects that occur during pedogenesis and microbial processing [*Benner et al*., 1987; *Bowen and Beerling*, 2004; *Natelhoffer and Fry*, 1988; *Schmidt et al*., 2011; *Schweizer et al*., 1999; *Wynn*, 2007].

[36] Local variation in input and preservation/degradation of organic material may obscure the identification and accurate correlation of even large isotopic shifts such as the recovery of the CIE. The observed truncation of the body of the CIE in bulk organic matter could potentially lead to false correlations, misidentification of the PETM recovery phase, and significant (30–80%) underestimations of the thickness of PETM strata. Smaller magnitude shifts in $\delta^{13}C_{org}$ values are not likely to be reliable for correlation, even for stratigraphic sections that are relatively close together like ours. Only the onset of the CIE appears to be a shift large enough to overwhelm local heterogeneity, and without dense sampling, even the onset of the CIE can be difficult to identify.

5.3.2. Proximal Correlations: The Adjacent Honeycombs Section

[37] A vertebrate microsite near North Butte in the Honeycombs badland area of the SE Bighorn Basin (Figures 1 and 2) contains mammal species indicative of the Wa-0 faunal zone [*Strait*, 2001, 2003]. *Yans et al*. [2006] conducted a chemostratigraphic study in the vicinity of the microsite, producing a $\delta^{13}C_{org}$ profile through the PETM using protocols similar to those we have used (Figure 5). They identified the onset of the CIE as a −3.7‰ excursion between the 7.8 and 8.5 m levels in their stratigraphic section and offered a possible correlation of four negative isotope landmarks between the Honeycombs and Polecat Bench $\delta^{13}C_{org}$ records by aligning the base of the CIEs. The Honeycombs CIE identified by *Yans et al*. [2006] approximately matches the Polecat Bench $\delta^{13}C_{org}$ excursion in both magnitude and stratigraphic thickness, and a Wa-0 fauna is preserved within the Honeycombs CIE [*Strait*, 2001, 2003].

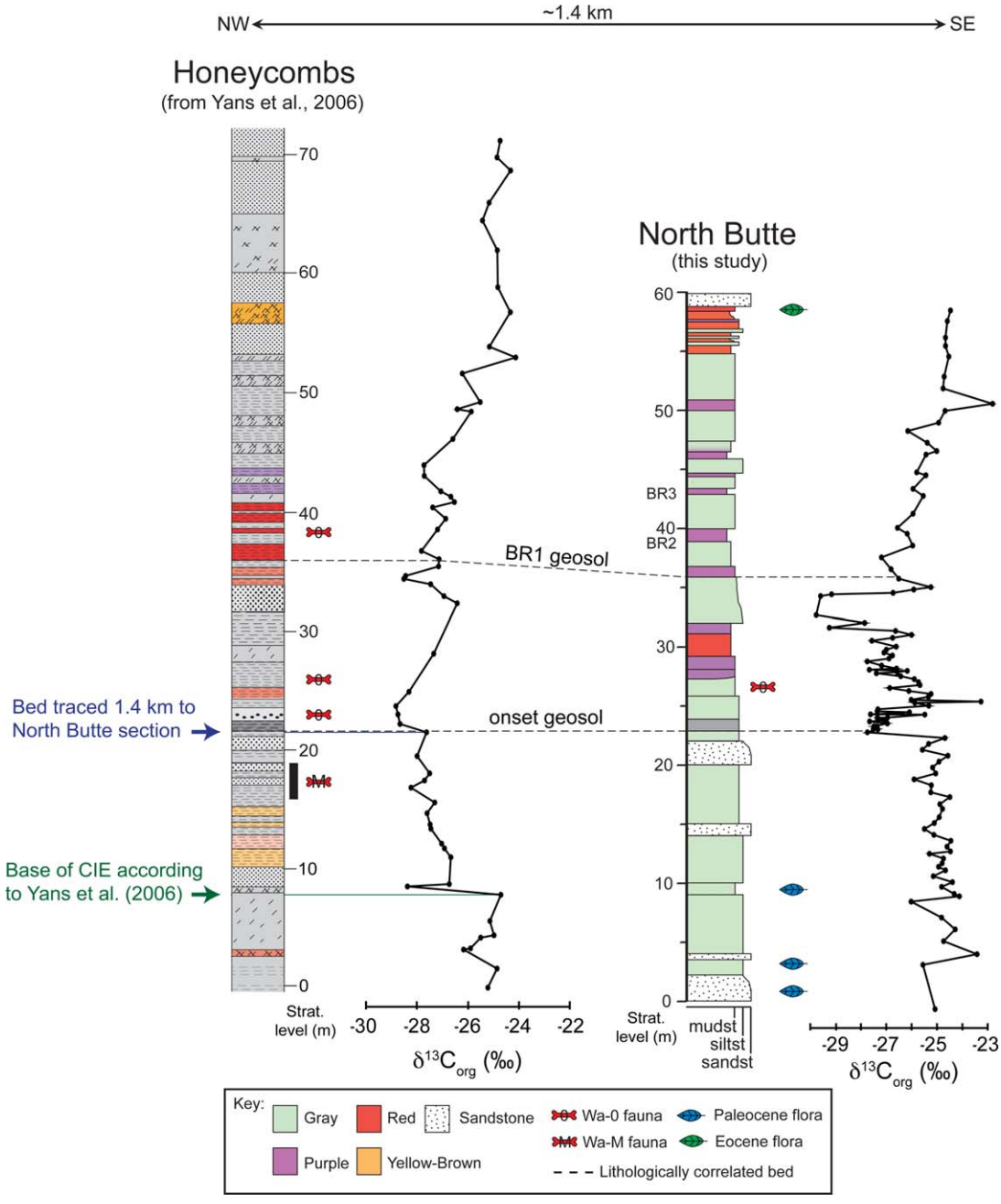

Figure 5. Lithostratigraphic correlation of the Honeycombs section of *Yans et al*. [2006] with the North Butte section (this study). The two sections were correlated lithostratigraphically by following the "gray tracer" marker bed at ~21.5 m of the Honeycombs section [*Yans et al*., 2006] southeast 1.4 km to the ~23 m level of the North Butte section. The "gray tracer" bed of *Yans et al*. [2006], here called the onset geosol, was also followed westward in outcrop from North Butte to the Pyramid Point, Big Red Spit, CAB 3, CAB 10, and HW 16 sections. Green line indicates the onset of the CIE identified in *Yans et al*. [2006].

[38] Comparison of the Honeycombs section to our sites in the SE Bighorn Basin, however, indicates a revised position for the base of the CIE in the Honeycombs section (Figure 5). A DGPS trace of marker geosols from the Honeycombs section to the sections we have measured shows that the "gray tracer" bed of *Yans et al*. [2006] is the same as our onset geosol, and the "thick red" of *Yans et al*. [2006] is the same as our BR1 geosol (Figure 2 and Table 2). These equivalences are most apparent in traces between the Honeycombs section and the North Butte section 1.4 km to the

Table 2. Summary of Papers Referring to Beds That Are Stratigraphically Equivalent to the Onset and BR1 Geosols

Source	Stratigraphic Equivalent	Meter Level (Base)	Comments on Equivalence
Onset geosol			
Wing et al. [2005]	(Not named but identified in stratigraphic column)	~0 m	Earliest identification of CIE in the field area at this level
Wing et al. [2009]	First laterally persistent red paleosol containing $CaCO_3$ nodules	Multiple sections[a]	Base of first laterally persistent red is base of onset geosol within field area
Chester et al. [2010]	(Not named but identified in stratigraphic column)	~0 m	Same stratigraphic column as *Wing et al*. [2005]
Secord et al. [2012]	LIRB (Lowest Intermittent Red Bed)	~14 m	Base of LIRB is base of onset geosol in composite section tied to CAB 10
Kraus et al. [2013]	(Not named but identified in stratigraphic column)	~20 m	Fine scale stratigraphic description of onset geosol at HW 16
Yans et al. [2006]	Gray tracer	~22 m	Traced laterally between Honeycombs section and our field area using DGPS
Kraus and Riggins [2007]	1st Persistent Red	0 m	Traced through intermittent outcrops to onset geosol at HW 16
Rose et al. [2012]	Red 1	0 m	Traced through intermittent outcrops to onset geosol at HW 16; supported by biostratigraphy
BR1 geosol			
Wing et al. [2005]	(Not named but identified in stratigraphic column)	~35 m	Earliest identification of big red sequence in field area
Wing et al. [2009]	Lowest red paleosol in the big red sequence	Multiple sections[a]	Earliest identification of BR1 within field area
Chester et al. [2010]	(Not named but identified in stratigraphic column)	~35 m	Same stratigraphic column as *Wing et al*. [2005]
Secord et al. [2012]	BR1 (Big Red 1)	~42 m	BR1 within composite section tied to CAB 10
Kraus et al. [2013]	(Not named but identified in stratigraphic column)	~50 m	Fine scale stratigraphic description of big red sequence at HW 16
Yans et al. [2006]	Thick red	~37 m	Traced laterally between Honeycombs section and our field area using DGPS
Kraus and Riggins [2007]	Big Red Paleosol	~18 m	Traced through intermittent outcrops to BR1 geosol at HW 16
Rose et al. [2012]	Big Red	~23 m (S); ~17 m (N)	Traced through intermittent outcrops to BR1 geosol at HW 16; supported by biostratigraphy

[a]Candystripe Ridge and Picnic Area Hill [*Wing et al*., 2009] together comprise the HW 16 section presented in Figure 3. Big Red Spit [*Wing et al*., 2009] is the Pyramid Point section in Figure 3 of this study.

southeast (Figure 5). The base of the CIE proposed by *Yans et al*. [2006] is 13.6 m below the onset geosol that records the onset of the CIE in our six sections in the SE Bighorn Basin.

[39] This revised position for the base of the CIE in the Honeycombs section corresponds to an isotopic shift of only −1.2‰ (Figure 5), but it is not discordant with any of the biostratigraphic data presented by *Yans et al*. [2006]. The lowest Wa-0 mammal fossils are from the Castle Gardens and Halfway Hill S localities, ~1–2 m above the base of gray tracer [*Strait*, 2001; *Yans et al*., 2006]. The stratigraphically highest Wa-0 fossils in the Honeycombs section are within the thick red paleosol, which is our BR1 geosol (Table 2), a paleosol that also contains Wa-0 mammals in our sections (Figures 3 and 5) [*Secord et al*., 2012; *Wing et al*., 2005]. *Yans et al*. [2006] reported a single specimen of *Meniscotherium*, the index fossil for biozone Wa-M, ~2–5 m below gray tracer. At Polecat Bench in the northern Bighorn Basin, *Meniscotherium* coincides with minimum CIE values, below the first Wa-0 mammals but above the onset of the CIE [*Bains et al*., 2003; *Bowen et al*., 2001; *Gingerich*, 2003; *Gingerich and Smith*, 2006; *Magioncalda et al*., 2004]. The stratigraphic position of the *Meniscotherium* specimen from the Honeycombs section, ~2–5 m below where we place the base of the CIE, can be explained by a small amount of downslope movement of the specimen after it was eroded from the outcrop [*Wing et al*., 2009; *Wood et al*., 2008]. The onset geosol in this area is immediately underlain by a laterally extensive sandstone unit ~2–3 m thick, which forms a steeply weathered face. We have found many places where moderately abundant vertebrate fossils weathering out of the onset geosol have been washed down this steep face and come to rest on nearly horizontal surfaces just below [*Chester et al*., 2010; *Wing et al*., 2009]. The revised position of the onset of the CIE in the Honeycombs section casts doubt on the

correlations of the smaller isotopic landmarks proposed between Honeycombs and Polecat Bench [*Yans et al*., 2006].

5.3.3. Basinwide Comparisons: Sand Creek Divide and Polecat Bench

[40] The sequence of paleosols at the Sand Creek Divide PETM locality [*Rose et al*., 2012], ~19 km northwest of HW 16 (Figures 1 and 2), is similar to the paleosol sequence in the SE Bighorn Basin (Figure 4). We tentatively identify the onset geosol as the gray paleosol immediately underlying the lowest persistent red paleosol [*Rose et al*., 2012, "Red 1"], which marks the base of the Willwood Fm and contains the lowest pedogenic carbonate nodules (Figure 4 and Table 2) [*Rose et al*., 2012]. Red 1 is overlain by a prominent gray mudstone [*Rose et al*., 2012, Figures 2A and B], forming a gray-red-gray sequence similar to that in the HW 16 section (Figure 4). We also tentatively identify the BR1 geosol as the "Big Red" paleosol of *Rose et al*. [2012] (Table 2). Although the sequence of paleosols at the more distant Polecat Bench [*Bowen et al*., 2001; *Gingerich*, 1989, 2001; *Magioncalda et al*., 2004] in the northern Bighorn Basin (Figure 1) is different enough to impede lithostratigraphic correlation, biostratigraphic and chemostratigraphic evidence for the PETM enables us to compare and contrast the carbon isotope record from the Polecat Bench section with those from the SE Bighorn Basin (Figure 4).

[41] Both the Polecat Bench and Sand Creek Divide $\delta^{13}C_{org}$ profiles have thicker CIE onset intervals relative to sites in the SE Bighorn Basin (Figure 4). In the northern Bighorn Basin, the $\delta^{13}C_{org}$ record at Polecat Bench shifts −3.7‰ over 3.9 m [*Magioncalda et al*., 2004, Figure 2 and Table DR1]. At Sand Creek Divide, the coarse sampling resolution prevents a precise estimate of the thickness over which the onset occurs, but the shift spans at least several meters of section and is more gradual [*Rose et al*., 2012] than at sites to the southeast where the onset occurs over <2 m [this study; *Yans et al*., 2006]. Therefore, in general, the CIE onset interval recorded in bulk organic matter thins southeastward across the entire Bighorn Basin, from Polecat Bench in the north to the sections in this study and the Honeycombs site [*Yans et al*., 2006] at the southeastern margin of the basin (Figure 1). Likewise, the body of the PETM, defined by lithostratigraphy and biostratigraphy, also thins to the SE margin of the Bighorn Basin; from ~40 m at Polecat Bench to ~32 m at Sand Creek to <32 m in our field area in the SE Bighorn Basin (Figure 4).

[42] Comparison of the PETM sections provides insight into spatial differences in sedimentation rates across the Bighorn Basin. However, because of the landscape scale variations observed in the $\delta^{13}C_{org}$ curves in this study, we caution against correlations among distant sites based on shifts in isotope ratios from bulk organic matter within the PETM.

5.3.4. Ecological, Evolutionary, and Carbon Cycle Changes at the PETM

[43] Marine carbonate records of the CIE often display truncation due to dissolution caused by the shoaling of the lysocline [*McCarren et al*., 2008; *Zachos et al*., 2005]. In contrast, terrestrial records are often considered to more completely preserve the CIE [*McInerney and Wing*, 2011]. The data presented here demonstrate that bulk organic matter $\delta^{13}C$ profiles recorded in soils and floodplain sediments can also suffer from incomplete preservation of the CIE and can underrepresent both the thickness of the PETM body and the magnitude of the CIE. This influences mass balance approaches to modeling the amount of carbon that fueled the global warming at the Paleocene-Eocene boundary, which rely on the magnitude of the CIE [See *McInerney and Wing*, 2011 for review] and hypotheses regarding source(s), mechanism(s), and rate of carbon release. Variation in the magnitude and shape of the CIE across the field area demonstrates the importance of local processes and suggests that bulk organic matter cannot be reliably used to infer the shape or magnitude of the global CIE in areas where allochthonous organic matter could have been a significant contributor to the sedimentary organic carbon pool.

[44] Truncation of the CIE in terrestrial bulk organic matter also has implications for the reconstruction of ecological and evolutionary responses to the PETM. Studies that rely solely on bulk organic matter CIEs risk assuming that a truncated CIE body represents the full ~100–120 kyr of the CIE body. The results presented here suggest that the CIE in bulk organic matter could underestimate the PETM body by 30–80%. In a worst case scenario, the observed CIE could represent only 20% of the actual PETM body, leading to the calculation of rates of migration, evolution, and sedimentation that are underestimated by a factor of 5. The estimation of rates of migration and evolution during the PETM has implications for anticipating future biotic responses to global warming.

6. Summary and Conclusions

[45] Six high-resolution bulk soil organic matter $\delta^{13}C$ records from a 16 km transect across a suite of ancient floodplains in the SE Bighorn Basin, Wyoming, have been correlated using floral and faunal biostratigraphy and by tracing distinctive lithologic marker beds that characterize the PETM. This multiproxy approach has established a comprehensive PETM stratigraphic framework with which we can carefully examine how local processes influence and overprint the global PETM signal. The onset of the CIE occurs within the prominent and laterally extensive onset geosol at all six sites, confirming for the first time that this important chemostratigraphic marker occurs in the same lithostratigraphic position across an ancient floodplain.

[46] Carbon isotope ratios in bulk organic matter underestimate the thickness of the body of the PETM (as indicated by floral and faunal biostratigraphy and stable carbon isotope measurements from pedogenic carbonate nodules, tooth enamel, and leaf wax lipids) by ~30%–80%. The premature recovery to less negative $\delta^{13}C_{org}$ values in the SE Bighorn Basin does not occur at the same level in relation to biostratigraphic and lithostratigraphic markers at each site, nor does it agree with $\delta^{13}C$ records from tooth enamel, leaf waxes, and carbonate nodules, which record a thicker CIE. As a result, $\delta^{13}C_{org}$ records could lead to false correlations of the CIE recovery, underestimations of the thickness of PETM strata, and the miscalculation of rates of sedimentation, evolution, and migration.

[47] We suggest that the discrepancy between the $\delta^{13}C_{org}$ records and the biostratigraphic and isotopic records from other proxies is caused by erosion of older rocks and redeposition of allochthonous carbon in this PETM floodplain environment, similar to that observed in modern fluvial systems. According to this hypothesis, the contribution of older allochthonous organic matter reduced the overall magnitude of the CIE in the $\delta^{13}C_{org}$ record. Stratigraphic fluctuations in the ratio of allochthonous to autochthonous carbon are responsible for oscillations in the bulk organic matter $\delta^{13}C$ record for each local section, and an increase in the ratio caused the body of the CIE to appear truncated. The minimum proportion of allochthonous carbon required to explain the truncation of the CIE ranges from 40 to 80%, which is in agreement with observations in modern floodplain settings. The variability in $\delta^{13}C_{org}$ ratios within a single record and the differences in CIE shape across our field area demonstrate the importance of local environmental, biogeochemical, and/or sedimentological factors in determining $\delta^{13}C_{org}$ values in terrestrial floodplain environments, particularly where abundant allochthonous organic matter has been eroded from older rocks and redeposited during the CIE. These strong local controls mean that a single $\delta^{13}C_{org}$ curve may not be representative of even a relatively restricted field area, let alone an entire basin or continent. Multiple, high-resolution records across a field area with biostratigraphic and lithostratigraphic constraints can provide more robust identification of the PETM. Within such a stratigraphic framework, the nature of the CIE preserved in bulk organic matter can be examined to answer questions about carbon cycle dynamics among the atmosphere, terrestrial ecosystems, and soils during the PETM.

Acknowledgments

[48] We thank Alexa Socianu for help with carbonate isotope laboratory work, Stephen Chester for assisting with biostratigraphic and lithostratigraphic studies, Brady Foreman and Elizabeth Denis for sample collection, and the many students and volunteers who helped with fieldwork and laboratory work. We also thank two anonymous reviewers for their constructive comments. Funding was provided by NSF awards EAR-0720268 (F.A.M.), EAR-0717892 (S.L.W.), EAR-0718740 (M.J.K.), EAR-0719941 (J.I.B.), EAR-0640076 (J.I.B., R.S., and John Krigbaum), Initiative for Sustainability and Energy at Northwestern (F.A.M.), and Australian Research Council FT110100793 (F.A.M.). Vertebrate fossils were collected under Bureau of Land Management permits to J.I.B. (PA04-WY-113, PA10-WY-185). A portion of this manuscript was written when J.I.B. was supported as an Edward P. Bass Distinguished Visiting Environmental Scholar in the Yale Institute for Biospheric Studies (YIBS).

References

Abdul Aziz, H., F. J. Hilgen, G. M. van Luijk, A. Sluijs, M. J. Kraus, J. M. Pares, and P. D. Gingerich (2008), Astronomical climate control on paleosol stacking patterns in the upper Paleocene-lower Eocene Willwood Formation, Bighorn Basin, Wyoming, *Geology*, *36*(7), 531–534.

Bains, S., R. D. Norris, R. M. Corfield, G. J. Bowen, P. D. Gingerich, and P. L. Koch (2003), Marine-terrestrial linkages at the Paleocene-Eocene boundary, *in*: Causes and Consequences of Globally Warm Climates in the Early Paleogene, edited by Wing, S. L., Gingerich, P. D., Schmitz, B., and Thomas, E., pp. 1–9, The Geological Society of America Special Paper 369. Boulder, CO.

Benner, R., M. L. Fogel, E. K. Sprague, and R. E. Hodson (1987), Depletion of ^{13}C in lignin and its implications for stable carbon isotope studies, *Nature*, *329*(6141), 708–710.

Blair, N. E., E. L. Leithold, H. Brackley, N. Trustrum, M. Page, and L. Childress (2010), Terrestrial sources and export of particulate organic carbon in the Waipaoa sedimentary system: Problems, progress and processes, *Mar. Geol.*, *270*(1–4), 108–118.

Bowen, G. J., and D. J. Beerling (2004), An integrated model for soil organic carbon and CO_2: Implications for paleosol carbonate pCO_2 paleobarometry, *Global Biogeochem. Cycles*, *18*, GB1026, doi:10.1029/2003GB002117.

Bowen, G. J., P. L. Koch, P. D. Gingerich, R. D. Norris, S. Bains, and R. Corfield (2001), Refined isotope stratigraphy across the continental Paleocene-Eocene boundary on Polecat Bench in the Northern Bighorn Basin, *In:* Paleocene-Eocene Stratigraphy and Biotic Change in the Bighorn and Clarks Fork Basins, Wyoming, edited by Gingerich, P. D., pp. 73–88, Univ. of Mich., Ann Arbor.

Bowen, G. J., et al. (2006), Eocene hyperthermal event offers insight into greenhouse warming, *Eos Trans. AGU*, *87*(17), 165–169.

Bown, T. M. (1980), Summary of latest Cretaceous and Cenozoic sedimentary, tectonic, and erosional events, Bighorn Basin, Wyoming, in *Early Cenozoic Paleontology and Stratigraphy of the Bighorn Basin, Wyoming*, edited by P. D. Gingerich, pp. 25–32, Univ. of Mich., Ann Arbor.

Brackley, H. L., N. E. Blair, N. A. Trustrum, L. Carter, E. L. Leithold, E. A. Canuel, J. H. Johnston, and K. R. Tate (2010), Dispersal and transformation of organic carbon across an episodic, high sediment discharge continental margin, Waipaoa Sedimentary System, New Zealand, *Mar. Geol.*, *270*(1–4), 202–212.

Charles, A. J., D. J. Condon, I. C. Harding, H. Paelike, J. E. A. Marshall, Y. Cui, L. Kump, and I. W. Croudace (2011), Constraints on the numerical age of the Paleocene-Eocene boundary, *Geochem. Geophys. Geosyst.*, *12*, Q0AA17, doi:10.1029/2010GC003426.

Chester, S. G. B., J. I. Bloch, R. Secord, and D. M. Boyer (2010), A new small-bodied species of *Palaeonictis* (Creodonta, Oxyaenidae) from the Paleocene-Eocene Thermal Maximum, *J. Mammalian Evol.*, *17*(4), 227–243.

Cierjacks, A., B. Kleinschmit, M. Babinsky, F. Kleinschroth, A. Markert, M. Menzel, U. Ziechmann, T. Schiller, M. Graf, and F. Lang (2010), Carbon stocks of soil and vegetation on Danubian floodplains, *J. Plant Nutr. Soil Sci.*, *173*(5), 644–653.

Clark, K. E., R. G. Hilton, A. J. West, Y. Malhi, D. R. Gröcke, C. L. Bryant, P. L. Ascough, A. Robles Caceres, and M. New (2013), New views on ''old'' carbon in the Amazon River: Insight from the source of organic carbon eroded from the Peruvian Andes, *Geochem. Geophys. Geosyst.*, *14*, 1644–1659, doi:10.1002/ggge.20122.

Clyde, W. C., and P. D. Gingerich (1998), Mammalian community response to the latest Paleocene thermal maximum: An isotaphonomic study in the northern Bighorn Basin, Wyoming, *Geology*, *26*(11), 1011–1014.

Clyde, W. C., W. Hamzi, J. A. Finarelli, S. L. Wing, D. Schankler, and A. Chew (2007), Basin-wide magnetostratigraphic framework for the Bighorn Basin, Wyoming, *Geol. Soc. Am. Bull.*, *119*(7–8), 848–859.

Crouch, E. M., C. Heilmann-Clausen, H. Brinkhuis, H. E. G. Morgans, K. M. Rogers, H. Egger, and B. Schmitz (2001), Global dinoflagellate event associated with the Late Paleocene Thermal Maximum, *Geology*, *29*(4), 315–318.

Crouch, E. M., G. R. Dickens, H. Brinkhuis, M. P. Aubry, C. J. Hollis, K. M. Rogers, and H. Visscher (2003), The Apectodinium acme and terrestrial discharge during the Paleocene-Eocene Thermal Maximum: New palynological, geochemical and calcareous nannoplankton observations at Tawanui, New Zealand, *Palaeogeogr. Palaeoclimatol. Palaeoecol.*, *194*(4), 387–403.

Cui, Y., L. R. Kump, A. J. Ridgwell, A. J. Charles, C. K. Junium, A. F. Diefendorf, K. H. Freeman, N. M. Urban, and I. C. Harding (2011), Slow release of fossil carbon during the Palaeocene-Eocene Thermal Maximum, *Nat. Geosci.*, *4*(7), 481–485.

Diefendorf, A. F., K. H. Freeman, S. L. Wing, and F. A. Smith (2007), Carbon-isotope variability in terrestrial environments: Examples from the Paleocene and Eocene sediments of the Bighorn Basin, Wyoming (USA), *Geol. Soc. of Am. Abstr. Programs*, *39*, 464.

Domingo, L., N. Lopez-Martinez, M. J. Leng, and S. T. Grimes (2009), The Paleocene-Eocene Thermal Maximum record in the organic matter of the Claret and Tendruy continental sections (South-central Pyrenees, Lleida, Spain), *Earth Planet. Sci. Lett.*, *281*(3–4), 226–237.

Dupuis, C., M. P. Aubry, E. Steurbaut, W. A. Berggren, K. Ouda, R. Magioncalda, B. S. Cramer, D. V. Kent, R. P. Speijer, and C. Heilmann-Clausen (2003), The Dababiya Quarry section: Lithostratigraphy, clay mineralogy, geochemistry and paleontology, *Micropaleontology*, *49*, 41–59.

Eicher, D. L. (1962), Biostratigraphy of the Thermopolis, Muddy, and Shell Creek Formations, in *Symposium on Early Cretaceous Rocks of Wyoming and Adjacent areas,* 17th Annual Field Conference Guidebook, edited by R.L. Enyert and W.H. Curry, pp. 72–93. Wyo. Geol. Assoc., Casper, WY.

Finn, T. M., M. A. Kirschbaum, S. B. Roberts, S. M. Condon, L. N. R. Roberts, and R. C. Johnson (2010), Cretaceous–Tertiary Composite Total Petroleum System (503402), Bighorn Basin, Wyoming and Montana, *U.S. Geol. Surv., Digital Data Ser. DDS-69-V*, 157 pp.

Fricke, H. C., W. C. Clyde, J. R. O'Neil, and P. D. Gingerich (1998), Evidence for rapid climate change in North America during the latest Paleocene thermal maximum: Oxygen isotope compositions of biogenic phosphate from the Bighorn Basin (Wyoming), *Earth Planet. Sci. Lett.*, *160*(1–2), 193–208.

Froehlich, D. J. (2002), Quo vadis eohippus? The systematics and taxonomy of the early Eocene equids (Perissodactyla), *Zool. J. Linnean Soc.*, *134*(2), 141–256.

Gingerich, P. D. (1989), New earliest Wasatchian mammalian fauna from the Eocene of northwestern Wyoming: Composition and diversity in a rarely sampled high-floodplain assemblage, *Univ. Mich. Pap. Paleontol.*, *28*, 1–97.

Gingerich, P. D. (2001), Biostratigraphy of the continental Paleocene-Eocene boundary interval on Polecat Bench in the northern Bighorn Basin, in *Paleocene-Eocene Stratigraphy and Biotic Change in the Bighorn and Clarks Fork Basins, Wyoming*, edited by P. D. Gingerich, pp. 37–71, Univ. of Mich., Ann Arbor.

Gingerich, P. D. (2003), Mammalian responses to climate change at the Paleocene-Eocene boundary: Polecat Bench record in the Northern Bighorn Basin, Wyoming, in: Causes and Consequences of Globally Warm Climates in the Early Paleogene, edited by Wing, S.L., Gingerich, P.D., Schmitz, B. and THomas, E., pp. 463–478, Geological Society of America Special Paper 369, Boulder, CO.

Gingerich, P. D., and T. Smith (2006), Paleocene-Eocene land mammals from three new latest Clarkforkian and earliest Wasatchian wash sites at Polecat Bench in the northern Bighorn Basin, Wyoming, *Contrib. Mus. Paleontol. Univ. Mich.*, *31*(11), 245–303.

Hagen, E. S., and R. C. Surdam (1984), Maturation history and thermal evolution of Cretaceous source rocks of the Bighorn Basin, Wyoming and Montana, in *Hydrocarbon Source Rocks of the Greater Rocky Mountain Region: Rocky Mountain Association of Geologists Guidebook*, edited by J. Woodward, F. F. Meissner, and J. L. Clayton, pp. 321–338. Rocky Mountain Assoc. Geol., Denver, CO.

Hickey, L. J. (1980), Paleocene stratigraphy and flora of the Clark's Fork Basin, in: Early Cenozoic Paleontology and Stratigraphy of the Bighorn Basin, Wyoming, edited by Gingerich, P.D., pp. 33–49, Univ. of Mich., Ann Arbor.

Hill, A. R., and M. Cardaci (2004), Denitrification and organic carbon availability in riparian wetland soils and subsurface sediments, *Soil Sci. Soc. Am. J.*, *68*(1), 320–325.

Hoffmann, T., S. Glatzel, and R. Dikau (2009), A carbon storage perspective on alluvial sediment storage in the Rhine catchment, *Geomorphology*, *108*(1–2), 127–137.

Keefer, W. R. (1972), Frontier, Cody, and Mesaverde Formations in the Wind River and southern Bighorn basins, Wyoming, *U.S. Geol. Surv. Prof. Pap. 495-E*, E1–E23.

Kennett, J. P., and L. D. Stott (1991), Abrupt deep-sea warming, palaeoceanographic changes and benthic extinctions at the end of the Palaeocene, *Nature*, *353*, 225–229.

Koch, P. L., J. C. Zachos, and P. D. Gingerich (1992), Correlation between isotope records in marine and continental carbon reservoirs near the Paleocene/Eocene boundary, *Nature*, *358*(6384), 319–322.

Koch, P. L., J. C. Zachos, and D. L. Dettman (1995), Stable-isotope stratigraphy and paleoclimatology of the Paleogene Bighorn Basin (Wyoming, USA), *Palaeogeogr. Palaeoclimatol. Palaeoecol.*, *115*(1–4), 61–89.

Koch, P. L., W. C. Clyde, R. P. Hepple, M. L. Fogel, S. L. Wing, and J. C. Zachos (2003), Carbon and oxygen isotope records from paleosols spanning the Paleocene-Eocene boundary, Bighorn Basin, Wyoming, in: Causes and Consequences of Globally Warm Climates in the Early Paleogene, edited by Wing, S.L., Gingerich, P.D., Schmitz, B., and THomas, E., pp. 49–64, Geological Society of America Special Paper 369, Boulder, CO.

Kraus, M. J. (1992), Alluvial response to differential subsidence—Sedimentological analysis aided by remote-sensing, Willwood Formation (Eocene), Bighorn Basin, Wyoming, USA, *Sedimentology*, *39*(3), 455–470.

Kraus, M. J., and S. Riggins (2007), Transient drying during the Paleocene-Eocene Thermal Maximum (PETM): Analysis of paleosols in the Bighorn Basin, Wyoming, *Palaeogeogr. Palaeoclimatol. Palaeoecol.*, *245*(3–4), 444–461.

Kraus, M. J., F. A. McInerney, S. L. Wing, R. Secord, A. A. Baczynski, and J. I. Bloch (2013), Paleohydrologic response to continental warming during the Paleocene-Eocene Thermal Maximum, Bighorn Basin, Wyoming, *Palaeogeogr. Palaeoclimatol. Palaeoecol*., *370*, 196–208.

Love, J. D., and A. C. Christiansen (1985), Geologic Map of Wyoming, U.S Geological Survey, Denver, CO.

Magioncalda, R., C. Dupuis, T. Smith, E. Steurbaut, and P. D. Gingerich (2004), Paleocene-Eocene carbon isotope excursion in organic carbon and pedogenic carbonate: Direct comparison in a continental stratigraphic section, *Geology*, *32*(7), 553–556.

Manners, H. R., et al. (2013), Magnitude and profile of organic carbon isotope records from the Paleocene–Eocene Thermal Maximum: Evidence from northern Spain, *Earth Planet. Sci. Lett.*, *376*, 220–230, doi:10.1016/j.epsl.2013.06.016.

McCarren, H., E. Thomas, T. Hasegawa, U. Rohl, and J. C. Zachos (2008), Depth dependency of the Paleocene-Eocene carbon isotope excursion: Paired benthic and terrestrial biomarker records (Ocean Drilling Program Leg 208, Walvis Ridge), *Geochem. Geophys. Geosyst.*, *9*, Q10008, doi:10.1029/2008GC002116.

McInerney, F. A., and S. L. Wing (2011), The Paleocene-Eocene Thermal Maximum: A perturbation of carbon cycle, climate, and biosphere with implications for the future, *Annu. Rev. Earth Planet. Sci.*, *39*, 489–516.

Murphy, B. H., K. A. Farley, and J. C. Zachos (2010), An extraterrestrial 3He-based timescale for the Paleocene-Eocene thermal maximum (PETM) from Walvis Ridge, IODP Site 1266, *Geochim. Cosmochim. Acta*, *74*(17), 5098–5108.

Natelhoffer, K. J., and B. Fry (1988), Controls on natural nitrogen-15 and carbon-13 abundances in forest soil organic matter, *Soil Sci. Soc. Am. J.*, *52*, 1633–1640.

Neasham, J. W., and C. F. Vondra (1972), Stratigraphy and petrology of lower Eocene Willwood Formation, Bighorn Basin, Wyoming, *Geol. Soc. Am. Bull.*, *83*(7), 2167–2180.

Newbury, S. S. (2011), *The sedimentary response to climate change during the Paleocene-Eocene Thermal Maximum, southeastern Bighorn Basin, Wyoming, USA*, Unpublished MS thesis, 91 pp., Univ. of Colorado, Boulder.

North American Commission on Stratigraphic Nomenclature (2005), North American stratigraphic code, *Am. Assoc. Petrol. Geol. Bull.*, *89*(11), 1547–1591.

Pagani, M., N. Pedentchouk, M. Huber, A. Sluijs, S. Schouten, H. Brinkhuis, J. S. S. Damste, G. R. Dickens, and E. Scientists (2006), Arctic hydrology during global warming at the Palaeocene/Eocene Thermal Maximum, *Nature*, *442*(7103), 671–675.

Rohl, U., T. Westerhold, T. J. Bralower, and J. C. Zachos (2007), On the duration of the Paleocene-Eocene thermal maximum (PETM), *Geochem. Geophys. Geosyst.*, *8*, Q12002, doi:10.1029/2007GC001784.

Rose, K. D., A. E. Chew, R. H. Dunn, M. J. Kraus, H. C. Fricke, and S. P. Zack (2012), Earliest Eocene mammalian fauna from the Paleocene-Eocene Thermal Maximum at Sand Creek Divide, Southern Bighorn Basin, Wyoming, *Univ. Mich. Pap. Paleontol.*, *36*, 1–122.

Samaritani, E., et al. (2011), Heterogeneity of soil carbon pools and fluxes in a channelized and a restored floodplain section (Thur River, Switzerland), *Hydrol. Earth Syst. Sci.*, *15*(6), 1757–1769.

Schmitz, B., and V. Pujalte (2007), Abrupt increase in seasonal extreme precipitation at the Paleocene-Eocene boundary, *Geology*, *35*(3), 215–218.

Schmidt, M. W. I., et al. (2011), Persistence of soil organic matter as an ecosystem property, *Nature*, *478*(7367), 49–56.

Schweizer, M., J. Fear, and G. Cadisch (1999), Isotopic (^{13}C) fractionation during plant residue decomposition and its implications for soil organic matter studies, *Rapid Commun. Mass Spectrom.*, *13*(13), 1284–1290.

Secord, R. (2008), The Tiffanian land-mammal age (middle and late Paleocene) in the northern Bighorn Basin, Wyoming, *Univ. Mich. Pap. Paleontol.*, *35*, 1–192.

Secord, R., P. D. Gingerich, M. E. Smith, W. C. Clyde, P. Wilf, and B. S. Singer (2006), Geochronology and mammalian biostratigraphy of middle and upper Paleocene continental strata, Bighorn Basin, Wyoming, *Am. J Sci.*, *306*(4), 211–245.

Secord, R., P. D. Gingerich, K. C. Lohmann, and K. G. MacLeod (2010), Continental warming preceding the Palaeocene-Eocene thermal maximum, *Nature*, *467*(7318), 955–958.

Secord, R., J. I. Bloch, S. G. B. Chester, D. M. Boyer, A. R. Wood, S. L. Wing, M. J. Kraus, F. A. McInerney, and J. Krigbaum (2012), Evolution of the earliest horses driven by climate change in the Paleocene-Eocene Thermal Maximum, *Science*, *335*(6071), 959–962.

Seeland, D. (1998), Late Cretaceous, Paleocene, and Early Eocene Paleogeography of the Bighorn Basin and Northwestern Wyoming, in *Cretaceous and Lower Tertiary Rocks of the Bighorn Basin, Wyoming and Montana*, 49th Annual Field Conference Guidebook, edited by Keefer W.R., and Goolsby J.E., pp. 137–165, Wyo. Geol. Assoc., Casper, WY.

Shrestha, J. (2011), *Spatiotemporal Variability of Carbon and Nitrogen in Floodplain Soils of a Perialpine River*, ETH Zurich.

Sluijs, A., J. Pross, and H. Brinkhuis (2005), From greenhouse to icehouse; organic-walled dinoflagellate cysts as paleoenvironmental indicators in the Paleogene, *Earth-Sci. Rev.*, *68*(3–4), 281–315.

Sluijs, A., et al. (2006), Subtropical Arctic Ocean temperatures during the Palaeocene/Eocene Thermal Maximum, *Nature*, *441*(7093), 610–613.

Sluijs, A., G. J. Bowen, H. Brinkhuis, L. J. Lourens, and E. Thomas (2007), The Palaeocene-Eocene Thermal Maximum super greenhouse: Biotic and geochemical signatures, age models and mechanisms of global change, in *Deep-Time Perspectives on Climate Change: Marrying the Signal from Computer Models and Biological Proxies*, edited by M. Williams, A. M. Haywood, F. J. Gregory, and D. N. Schmidt, pp. 323–349, The Micropalaeontol. Soc., Spec. Publ., The Geol. Soc., London, U. K.

Smith, F. A., S. L. Wing, and K. H. Freeman (2007), Magnitude of the carbon isotope excursion at the Paleocene-Eocene Thermal Maximum: The role of plant community change, *Earth Planet. Sci. Lett.*, *262*(1–2), 50–65.

Smith, J. J., S. T. Hasiotis, M. J. Kraus, and D. T. Woody (2008), Relationship of floodplain ichnocoenoses to paleopedology, paleohydrology, and paleoclimate in the Willwood Formation, Wyoming, during the Paleocene-Eocene Thermal Maximum, *Palaios*, *23*(9–10), 683–699.

Strait, S. G. (2001), New Wa-0 mammalian fauna From Castle Gardens in the southeastern Bighorn Basin, in: Paleocene-Eocene Stratigraphy and Biotic Change in the Bighorn and Clarks Fork Basins, Wyoming, edited by Gingerich, P.D., pp. 127–143, Univ. of Mich., Ann Arbor.

Strait, S. G. (2003), New mammalian fossils from the earliest Eocene (Wa-0), Bighorn Basin, Wyoming, *J. Vertebrate Paleontol. Abstr. Pap.*, *23*(supplement to 3), 101.

Thiry, M., M. P. Aubry, C. Dupuis, A. Sinha, L. D. Stott, and W. A. Berggren (2006), The Sparnacian deposits of the Paris Basin: $\delta^{13}C$ isotope stratigraphy, *Stratigraphy*, *3*(2), 119–138.

Thomas, E. (1989), Development of Cenozoic deep-sea benthic foraminiferal faunas in Antarctic waters, *Geol. Soc. London Spec. Publ.*, *47*, 283–296.

Thomas, E. (1998), Biogeography of the late Paleocene benthic foraminiferal extinction, *in*: Late Paleocene-Early Eocene Climatic and Biotic Events in the Marine and Terrestrial Records, edited by Aubry, M. P., Lucas, S., and Berggren, W.A., pp. 214–243, Columbia Univ. Press, New York.

Thomas, E., and N. J. Shackleton (1996), The Paleocene-Eocene benthic foraminiferal extinction and stable isotope anomalies, in: Correlation of the Early Paleogene in Northwest Europe, edited by Knox, R. W. O'B., Corfield, R. M., and Dunay, R. E., pp. 401–441, Geological Society, London, Special Publications 1996; v. 101; p. 401–441. doi: 10.1144/GSL.SP.1996.101.01.20

Tripati, A., and H. Elderfield (2005), Deep-sea temperature and circulation changes at the Paleocene-Eocene Thermal Maximum, *Science*, *308*(5730), 1894–1898.

Weijers, J. W. H., S. Schouten, A. Sluijs, H. Brinkhuis, and J. S. S. Damste (2007), Warm arctic continents during the Palaeocene-Eocene Thermal Maximum, *Earth Planet. Sci. Lett.*, *261*(1–2), 230–238.

Wing, S. L. (1998), Late Paleocene-Early Eocene floral and climatic change in the Bighorn Basin, Wyoming, in: Late Paleocene-Early Eocene Climatic and Biotic Events in the Marine and Terrestrial Records, edited by Aubry, M.P., Lucas, S., and Berggren, W.A., pp. 380–400, Columbia Univ. Press, New York.

Wing, S. L., and E. D. Currano (2013), Plant response to a global greenhouse event 56 million years ago, *Am. J. Bot.*, *100*(7), 1234–1254.

Wing, S. L., T. M. Bown, and J. D. Obradovich (1991), Early Eocene biotic and climatic-change in interior western North-America, *Geology*, *19*(12), 1189–1192.

Wing, S. L., G. J. Harrington, F. A. Smith, J. I. Bloch, D. M. Boyer, and K. H. Freeman (2005), Transient floral change and rapid global warming at the Paleocene-Eocene boundary, *Science*, *310*(5750), 993–996.

Wing, S. L., J. I. Bloch, G. J. Bowen, D. M. Boyer, S. Chester, A. F. Diefendorf, G. J. Harrington, M. J. Kraus, R. Secord, and F. A. McInerney (2009), Coordinated sedimentary and biotic change during the Paleocene-Eocene Thermal Maximum in the Bighorn Basin, Wyoming, USA, in *Climatic and Biotic Events of the Paleogene (CBEP 2009), Extended Abstracts From an International Conference in Wellington, New Zealand*, edited by E. M. Crouch, C. P. Strong, and C. J. Hollis, GNS Sci. Misc. Ser. *18*, pp. 156–162.

Wood, A. R., M. J. Kraus, and P. D. Gingerich (2008), Downslope fossil contamination: Mammal-bearing fluvial conglomerates and the Paleocene-Eocene faunal transition (Willwood Formation, Bighorn Basin, Wyoming), *Palaios*, *23*(5–6), 380–390.

Wynn, J. G. (2007), Carbon isotope fractionation during decomposition of organic matter in soils and paleosols: Implications for paleoecological interpretations of paleosols, *Palaeogeogr. Palaeoclimatol. Palaeoecol.*, *251*(3–4), 437–448.

Yans, J., S. G. Strait, T. Smith, C. Dupuis, E. Steurbaut, and P. D. Gingerich (2006), High-resolution carbon isotope stratigraphy and mammalian faunal change at the Paleocene-Eocene boundary in the Honeycombs area of the southern Bighorn Basin, Wyoming, *Am. J Sci.*, *306*(9), 712–735.

Zachos, J. C., K. C. Lohmann, J. C. G. Walker, and S. W. Wise (1993), Abrupt climate change and transient climates during the Paleogene: A marine perspective, *J Geol.*, *101*(2), 191–213.

Zachos, J. C., M. Pagani, L. Sloan, E. Thomas, and K. Billups (2001), Trends, rhythms, and aberrations in global climate 65 Ma to present, *Science*, *292*(5517), 686–693.

Zachos, J. C., M. W. Wara, S. Bohaty, M. L. Delaney, M. R. Petrizzo, A. Brill, T. J. Bralower, and I. Premoli-Silva (2003), A transient rise in tropical sea surface temperature during the Paleocene-Eocene Thermal Maximum, *Science*, *302*(5650), 1551–1554.

Zachos, J. C., et al. (2005), Rapid acidification of the ocean during the Paleocene-Eocene thermal maximum, *Science*, *308*(5728), 1611–1615.